Evolutionary origin of sex differentiation system in insects

Yasuhiko Chikami[1,2], Miki Okuno[3], Atsushi Toyoda[4,5], Takehiko Itoh[6], Teruyuki Niimi[1,2]*

[1]Division of Evolutionary Developmental Biology, National Institute for Basic Biology, 38 Nishigonaka, Myodaiji, Okazaki, Aichi, 444-8585, Japan

[2]Department of Basic Biology, School of Life Science, The Graduate University for Advanced Studies, SOKENDAI, 38 Nishigonaka, Myodaiji, Okazaki, Aichi, 444-8585, Japan

[3]Division of Microbiology, Department of Infectious Medicine, Kurume University School of Medicine, 67 Asahi-machi, Kurume, Fukuoka, 830-0011, Japan

[4]Comparative Genomics Laboratory, National Institute of Genetics, 1111 Yata, Mishima, Shizuoka 411-8540, Japan

[5]Advanced Genomics Center, National Institute of Genetics, 1111 Yata, Mishima, Shizuoka 411-8540, Japan

[6]School of Life Science and Technology, Tokyo Institute of Technology, 2-12-1 Ookayama, Meguro, Tokyo, 152-8550, Japan

***Corresponding author:**

Teruyuki Niimi

E-mail: niimi@nibb.ac.jp

This PDF file includes:

Main Text

Figures 1 to 6

Abstract

The evolution of the functionality of genes and genetic systems is a major source of animal diversity. Its best example is insect sex differentiation systems: promoting male and female differentiation (dual-functionality) or only male differentiation (single-functionality). However, the evolutionary origin of such functional diversity is largely unknown. Here, we investigate the ancestral functions of *doublesex*, a key factor of insect sex differentiation system, using the apterygote insect, *Thermobia domestica*, and reveal that its *doublesex* is essential for only males at the phenotypic level, but contributes to promoting female-specific *vitellogenin* expression in females. This functional discordance between the phenotypic and transcription-regulatory levels in *T. domestica* shows a new type of functionality of animal sex differentiation systems. Then, we examine how the sex differentiation system transited from the single-functionality to the dual-functionality in phenotypes and uncover that a conserved female-specific motif of *doublesex* is detected in taxa with the dual-functional *doublesex*. It is estimated that the role of the sex differentiation system for female phenotypes may have evolved through accumulating mutations in the protein motif structures that led to the enhancement of its transcription-regulatory function.

Introduction

Sex is a fundamental principle in animal reproduction and is shared among almost all animals. The differences between males and females are a large source of diversity in mating systems, species, traits, and ecological dynamics in Metazoa (*Darwin, 1871*; *Fryzell et al., 2019*; *Geddes and Thomson, 1889*). The universality of sex suggests that sex is an ancient feature of metazoans. On the other hand, recent studies in various animals have revealed that regulatory systems for producing sex change rapidly during animal evolution (*Bachtrog et al., 2014*; *Beukeboom and Perrin, 2014*; *Herpin and Schartl, 2015*). For example, genes in the sex determination/sex differentiation systems are more likely to change upstream in the gene cascade than downstream (*Bopp et al., 2014*; *Wilkins, 1995*). In eutherian mammals such as mice and humans, a transcription factor called *Sex-determining region Y* (*Sry*) acts as a 'master regulator' of sex determination pathway, in which *Sry* induces expression of a transcriptional factor *doublesex and mab-3 related transcriptional factor 1* (*dmrt1*) in males through chain reactions of transcription factors during embryogenesis (*Gubbay et al., 1990*; *Koopman et al., 1991*; *Miyawaki et al., 2020*; *Sinclair et al., 1991*). In contrast, in medaka fish, *Oryzias latipes*, a paralog of *dmrt1, dmy* (*DM-domain gene on the Y chromosome*) instead of *Sry* promotes male differentiation via a gene cascade inducing *dmrt1* (*Matsuda et al., 2002*; *Nanda et al., 2002*). The diversity in gene repertoires composing sex differentiation systems has also been found in arthropods (e.g., *Sharma et al., 2017*; *Suzuki et al., 2008*; *Xu et al., 2017*).

Diversity of sex differentiation systems has referred to differences in gene repertoires among species or populations. At present, many evolutionary scenarios

have been proposed to explain the evolutionary transition of gene repertoires in sex differentiation systems: e.g., neo-functionalization or sub-functionalization via gene duplication (e.g., *Chandler et al., 2017*; *Hattori et al., 2012*; *Hasselmann et al., 2008*; *Matsuda et al., 2002*; *Sharma et al., 2017*; *Yoshimoto et al., 2008*), positional exchange within the cascade via feedback loops (e.g., *Myosho et al. 2012*; *Myosho et al, 2015*; *Smith et al., 2009; Takehana et al., 2014*), and functional shifts via accumulation of mutations in *cis*- or *trans*-elements (e.g., *Kamiya et al., 2012*; *Sato et al., 2010*) (reviewed in *Beukeboom and Perrin, 2014*). Currently, most of the diversity of sex differentiation systems is explained by these well-understood scenarios for changes in gene repertoires. However, recently, a difference in sex differentiation systems without swapping gene repertoires has been discovered from pterygote insects.

Pterygote insects exhibit tremendous sexual dimorphisms in the head, abdomen, wings, and so on, realizing a complex mating strategy. Most of the sexual differences are produced by a sex differentiation system that uses a transcription factor *doublesex* (*dsx,* a homolog of *dmrt1*) as a bottom factor (*Kopp, 2012*; *Verhulst and van de Zande, 2015*). Studies on Aparaglossata (holometabolan insects excluding Hymenoptera) have shown that *dsx* promotes both male and female differentiation via the sex-specific splicing (*Burtis and Baker1989*; *Gotoh et al., 2016*; *Hildreth, 1964*; *Ito et al., 2013*; *Kijimoto et al., 2012*; *Ohbayashi et al., 2001*; *Shukla and Palli, 2012*; *Xu et al., 2017*). Recent studies showed that *dsx* promotes only male differentiation in several hemimetabolan and hymenopteran insects, even though *dsx* has sex-specific isoforms (*Mine et al., 2017*; *Takahashi et al., 2021*; *Wexler et al., 2015*; *Zhuo et al., 2018*). Thus, there is a difference in outputs in the sex differentiation systems in

92 insects: promoting only male differentiation (single-functionality) or both male and
93 female differentiation (dual-functionality). It is suggested that the output of the insect
94 sex differentiation systems transited from the single-functionality to the dual-
95 functionality (*Wexler et al., 2019*). However, it remains largely unclear how the
96 difference in the output evolved independently of changes in gene repertoires and
97 what drove such a transition (*Hopkins and Kopp, 2021*). Also, it is unidentified the
98 ancestral roles of *dsx* isoforms in insects.

99 The evolutionary origin of the sex differentiation system in insects is
100 ambiguous by the inability to estimate the status of the common ancestor of Insecta.
101 All of the previous studies examining the *dsx* functionality have been limited to
102 pterygote insects or crustaceans and chelicerates. In chelicerates and crustaceans, *dsx*
103 has no sex-specific isoforms (*Kato et al., 2011; Li et al., 2018; Panara et al., 2019;*
104 *Pomerantz et al., 2015*). We are currently forced to compare the status of crustaceans
105 with that of pterygote insects, resulting in a large gap in phylogenetic mapping.
106 Furthermore, previous reports of the single-functionality have been based mainly on
107 the sexual differences acquired or complicated by each taxon in hemimetabolan
108 insects. Therefore, it remains possible that the single-functionality reported so far
109 results in a secondary loss of roles in female differentiation.

110 To address these issues, it is necessary to examine the function of *dsx* in taxa
111 that retain the sexual traits of the common ancestor of Insecta and that emerged
112 between the crustaceans and Pterygota. To this end, we focused on the firebrat
113 *Thermobia domestica* (Zygentoma) belonging to Zygentoma, the sister group of
114 Pterygota (*Misof et al., 2014*). The sexual traits of *T. domestica* are restricted to the
115 female simple ovipositor and the male 'penis' that is not aedeagus. These sexual traits

mirror the ancestral state of insects (*Beutel et al., 2017*; *Boudinot, 2018*; *Emeljanov, 2014*; *Kristensen, 1975*; *Matsuda, 1976*). Here, to examine the exon-intron structure of *dsx*, we decoded the genome of *T. domestica*. Then, we developed the technology to effectively inhibit gene function during postembryonic development and investigated the roles of *dsx* for sexual traits, gametogenesis, and transcriptional regulation, and compared them with other insects.

Results

Molecular evolution of Doublesex in Pancrustacea

First, we examined the relationship among *dsx* homologs in animals (Figure1–figure supplement 1, Table 1) and revealed that the pancrustacean transcription factor *doublesex* (*dsx*) occurs in four clades: crustacean Dsx, Entognatha Dsx, Insect Dsx clade 1, and clade 2. (Figure 1A, B). *Thermobia domestica* has two *dsx* genes, belonging to different clades (Insect Dsx clade 1 and 2) (Figure 1–figure supplement 2). We considered the gene belonging to Insect Dsx clade 1 to be an ortholog of the pterygote *dsx*, since this clade contains Dsx of pterygote insects including *Drosophila melanogaster*. We thus named the gene in Insect Dsx clade 2 *dsx-like* to distinguish it from *dsx*. Insect Dsx clade 2 contained *dsx-like* in Zygentoma as well as Ephemeroptera and Phasmatodea (Figure 1B), indicating that *dsx* was duplicated before the emergence of the Dicondylia (= Zygentoma + Pterygota) and was lost repeatedly in pterygote taxa. This fact supports that *T. domestica* retains the ancestral state for *dsx* related genes' contents. Since these results suggested the involvement of

the gene duplication in the functional evolution of *dsx*, we also analyzed the expression and function of *dsx-like*.

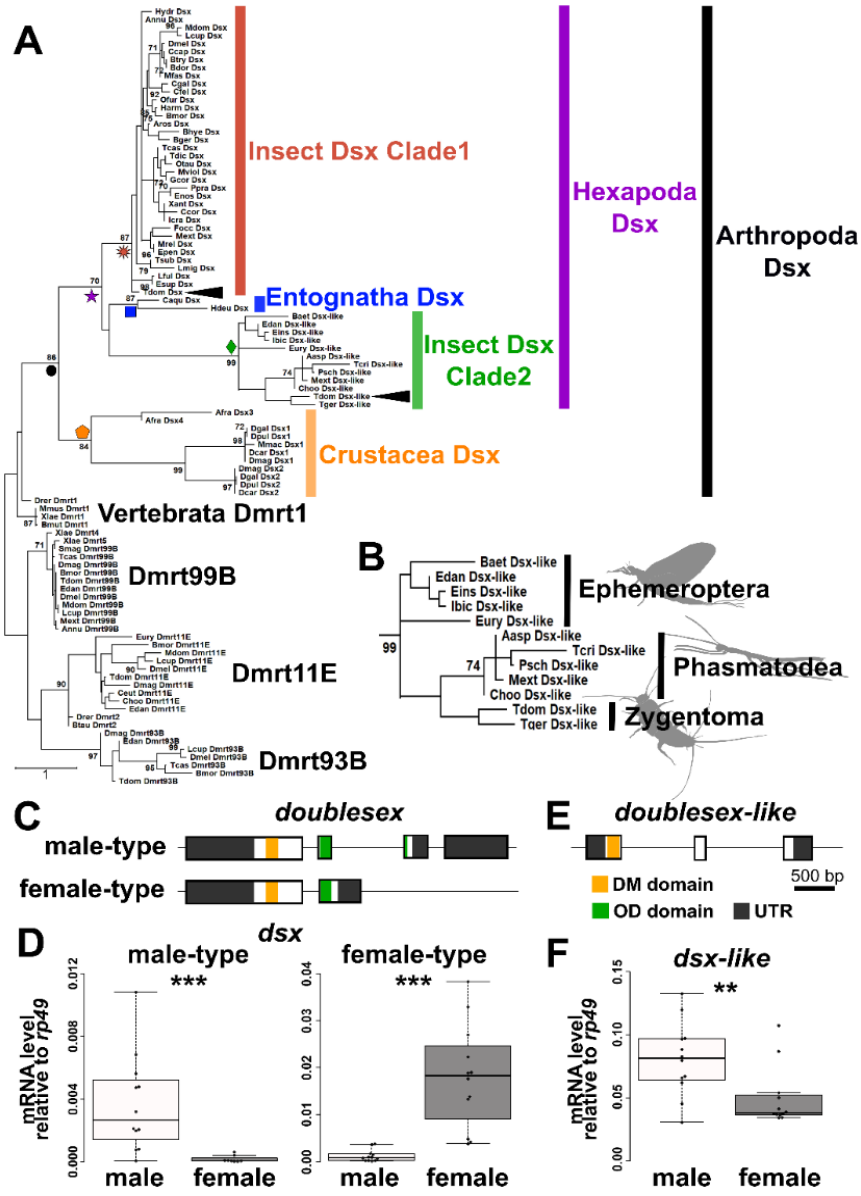

Figure 1. Molecular evolution and features of Doublesex in *Thermobia domestica*. (A to B) Molecular phylogeny of Doublesex and Mab-3 related transcriptional factors (DMRT) (A) and enlarged view of insect Dsx Clade2 (*dsx-like* clade) (B). The numerical value on each node is the bootstrap supporting value. Bootstrap values < 70 are not shown. The node of each clade is indicated by colored shapes: black circle, Arthropoda Dsx; orange pentagon, Crustacea Dsx; purple star, Hexapoda Dsx; red sunburst, Insect Dsx Clade1; green diamond, Insect Dsx Clade2; blue square, Entognatha Dsx. (C to F) Molecular features of *dsx* (C and D) and *dsx-like* (E and F). (C and E) indicate exon-intron structures of *dsx* and *dsx-like*, respectively. (D and F) show mRNA expression levels of *dsx* and *dsx-like*, respectively. Each plot is a value of an individual. Sample size is listed in Table 2. Results of Brunner–Munzel tests are indicated by asterisks: ***P*<0.01; ****P*<0.001 and are described in Table 2.

153 **Sex-specific splicing regulation of *doublesex* in *Thermobia domestica***

154 We detected two major isoforms of *dsx* of *T. domestica* (Figure 1C). Mapping
155 these sequences to our genome data showed that the longer (951 bp) and shorter (756
156 bp) isoforms. Both isoforms shared a Doublesex and Mab-3 (DM) domain-containing
157 exon, but differed in the 3'-terminus. The longer isoform was expressed at 40-fold
158 higher levels in males than in females in the fat body. The shorter isoform was
159 expressed in the fat body 18 times higher in females than in males (Figure 1D). We
160 named thus the longer and shorter isoforms *dsx* male-type and *dsx* female-type,
161 respectively. *dsx-like* was expressed two-fold more highly in males than in females
162 (Figure 1F) but had no isoform (Figure 1E). Thus, *dsx* was regulated by a sex-specific
163 splicing, whereas *dsx-like* was not under splicing control.

164 Before RNA interference (RNAi) analyses, we confirmed that expression
165 levels of *dsx* and *dsx-like* mRNA were significantly reduced in *dsx* and *dsx-like* RNAi
166 males and females. (Figure 1–figure supplement 3A and Table 2; see Materials and
167 Methods section).

168 **Single-functionality of *doublesex* for phenotypic sex differentiation in *T.***
169 ***domestica***

170 The sexual traits in *T. domestica* are the male penis and the female ovipositor
171 (Figure 2A–D).

172 In *T. domestica* males, the penis is an unpaired appendix on the abdomen
173 segment IX (*Matsuda, 1976*). The penis was sub-segmented into two parts. There
174 were many setae on the left and the right side of the distal tips (Figure 2E, Figure2–
175 figure supplement 1E). The surface of the penis had a reticulated pattern (Figure 2E,
176 Figure2–figure supplement 1C, E). This simple penial structure was presumably
177 gained at the last common ancestor of Ectognatha (*Boudinot, 2018*).

In *T. domestica* female, the ovipositor consists of two pairs of appendices (gonapophysis) and is derived from the retracted vesicles on the abdomen VIII and IX (*Emeljanov, 2014*; *Matsuda, 1976*). This ovipositor is an autapomorphy of Ectognatha (*Beutel, 2017*; *Kristensen, 1975*). The gonapophyses on the abdomen VIII (valvula I) were the ventral part of the ovipositor and a paired structure. The gonapophyses on the abdomen IX (valvula II) were the dorsal side of the ovipositor and were united to form an unpaired structure (Figure 2–figure supplement 2B). The distal tip of the valvula II remained a paired structure and possessed dense setae (Figure 2–figure supplement 2A). The valvula I was shorter than the valvula II (Figure 2–figure supplement 2A). Both valvulae were sub-segmented and have some setae (Figure 2F). The valvula I and II were connected through a tongue-and-groove structure (olistheter). The olistheter consisted of an aulax (”groove”) on the valvula I and a rhachis (”tongue”) on the valvula II (Figure 2–figure supplement 2B). Within the valvulae, the epithelial cells were beneath the cuticular layer. The cuticular layer was thickened and multi-layered in the outer surface of the ovipositor. In contrast, the inner surface (i.e., the side of the egg cavity) of the ovipositor had a thin and single-layered cuticle.

In *dsx* or *dsx* male-type RNAi males, a tubular organ was formed instead of the penis (Figure 2C, Figure2–figure supplement 1A). This tubular organ consisted of two pairs of appendage-like structures. The inner one is connected to the gonopore and the ejaculatory duct. The outer one had a lot of setae on its tip (Figure 2E, Figure2–figure supplement 1C, E). Thus, the inner pair was similar to the valvula I of the female ovipositor and the outer one was similar to the valvula II. These features indicated that the tubular organ in the *dsx* RNAi males was parallel to the female ovipositor. The same phenotype was found in the *dsx* and *dsx-like* double RNAi

males. In contrast, the *dsx-like* males possessed a penis the same as that of the control insects.

In females that were treated with RNAi for *dsx*, *dsx* isoforms, *dsx-like*, or both genes, the external genital organ was the same as the ovipositor of the control females that described in the above section (Figure 2D, F, Figure 2–figure supplement 1B, D, F, Figure2–figure supplement 2). Thus, in the view of histology, the location, and the relation to other elements, the external organ of the RNAi females was not different from the ovipositor of the control ones.

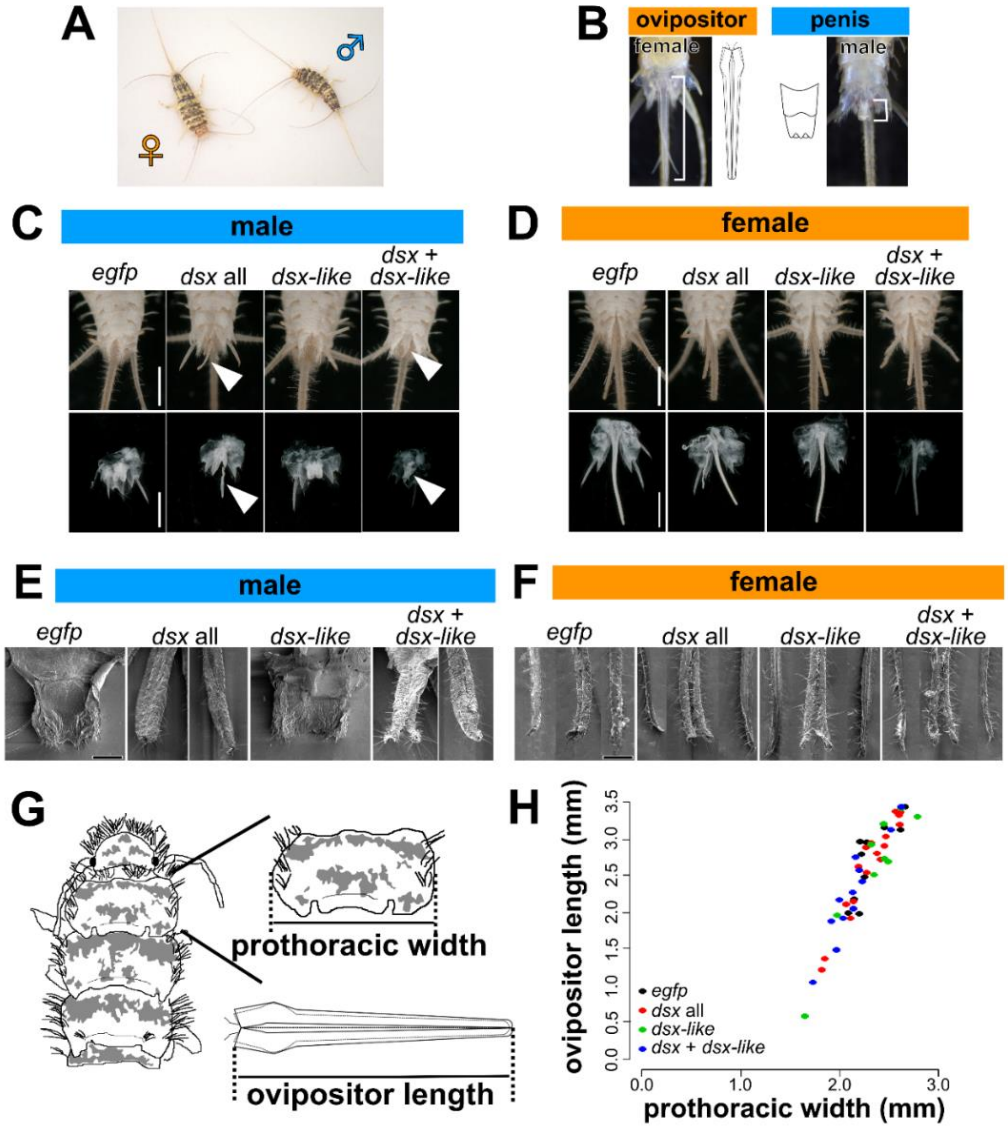

Figure 2. Function of Doublesex in sexually dimorphic traits in *Thermobia domestica*. (A) A pair of *T. domestica*. The female looks much the same as the male.

(B) Sexually dimorphic traits of *T. domestica*. Females possess an ovipositor and males have a penis. (C to F) Phenotypes of *dsx* and *dsx-like* RNA interference (RNAi) individuals. Light microscopic image (C and D) and scanning electron microscopic image (E and F). Scales: 1 cm (C and D); 50 μm (E and F). (G to H) Effect of *dsx* and *dsx-like* RNAi on the growth of the ovipositor. The ovipositor length was measured and is plotted with prothoracic width, an indicator of body size. The measurement scheme (G) and scatter plots (H). Each plot in (H) indicates a value of each individual. Sample size of (H) is listed in Table 4. Results of the generalized linear model analysis are listed in Table 4.

No evidence for the effects of *doublesex* on female phenotypes in *T. domestica*

To investigate whether *dsx* in *T. domestica* females has functions other than female differentiation for phenotypes, we examined its role in the growth and maintenance of female organs (Figure 2G). We did not detect a significant difference in ovipositor length and prothoracic width, an indicator of body size, between the controls and the *dsx* and *dsx-like* RNA females (Figures 2H, Figure 2–figure supplement 3, Figure2–figure supplement 4 and Table 4).

We then examined the effects of *dsx* on gonads, reproductive systems, and gametogenesis in *T. domestica*.

In males of *T. domestica*, a pair of testes was consisted of some testicular follicles (Figure 3A). Each testicular follicle was connected to the vas deferens via the vas efferens (Figure 3–figure supplement 1B). The seminal vesicle lay between the vas deferens and the ejaculatory duct. A pair of the ejaculatory ducts was associated with each other in the front of the gonopore in the penis (Figure 3C). The testicular follicles were a bean-like shape and the seminal vesicles were a bean pod-like shape. In the testicular follicle, the spermatogonia was in the antero-most part (Figures 3A). The primary and secondary spermatocytes lay in the middle part (Figures 3A). In the posterior part of the testicular follicle, there were some sperm bundles (Figures 3A). The wall of the testicular follicle consisted of a single flattened epithelial layer.

We observed the above features of the reproductive system in *dsx* or *dsx-like* RNAi males (Figure 3A and C). In *dsx* and both genes RNAi males, the seminal vesicles were round in shape. The vas efferens was filled with the sperm (Figure 3–figure supplement 1B). In contrast, we could not find differences in the morphology of the testicular follicles or spermatogenesis between the RNAi and control males. The male reproductive system and spermatogenesis showed no visible difference between *dsx* female-type and *dsx-like* RNAi females and the control ones.

In females of *T. domestica*, each ovary consists of five ovarioles and was attached to the anterior part of the abdomen via the terminal tuft (Figure 3–figure supplement 1). The ovarioles were associated with each other at the lateral oviduct. The lateral oviduct was connected to the common oviduct and subsequently opened at the gonopore in the valvula I. There was no vagina between the gonopore and the oviduct. The spermatheca was located on the branch point of the common oviduct along the midline (Figure 3–figure supplement 1A). The spermatheca was divided into two parts: anterior and posterior (Figure 3–figure supplement 2). The anterior part consisted of a pseudostratified layer of the columnar epithelial cells that were secretory. The posterior part was surrounded by a single layer of epithelial cells. The ovariole was panoistic-type and was composed of two parts: the germarium and the vitellarium (Figure 3A, B). The germarium contained many oogonia and young oocytes. The vitellarium had previtellogenic and vitellogenic oocytes. The oocytes in the vitellarium were surrounded by a single layer of follicle cells. There were pedicel cells in the terminal of the ovariole. The previtellogenic oocyte had a large germinal vesicle and basophilic cytoplasm. The vitellogenic oocyte was elongated along the anterior-posterior axis of the ovariole and had eosinophilic cytoplasm. Many eosinophilic lipid droplets were present in the peripheral region of the vitellogenic

267 oocytes. The follicle cells were flattened and columnar in shape in the
268 previtellogenesis and the vitellogenesis.

269 We observed the above features of the reproductive system in *dsx* or *dsx-like*
270 RNAi females (Figures 3A, Figure 3–figure supplement 1, Figure 3–figure
271 supplement 2). We could not detect differences in the female reproductive system or
272 oogenesis between the RNAi females and the controls. This result suggests that the
273 *dsx* and *dsx-like* have no function in the formation of female traits and gametogenesis
274 at the tissue and cellular level.

275 Also, we were not able to detect any differences in the oocyte number and size
276 between the controls and RNAi females (Figures 3B, Figure3–figure supplement 3
277 and Table 4). However, the seminal vesicle in males became round in shape in the *dsx*
278 RNAi males in contrast to the bean pod-like shape observed in the control males
279 (Figures 3C, Figure3–figure supplement 1). We detected a significant reduction of the
280 number of sperms within the seminal vesicle in *dsx* RNAi males (Figure 3D and Table
281 5). *dsx* thus contributed to the development of the reproductive system and gametes in
282 males, but not in females, of *T. domestica*.

283 Our results cannot show evidence for roles of *dsx* in *T. domestica* females.

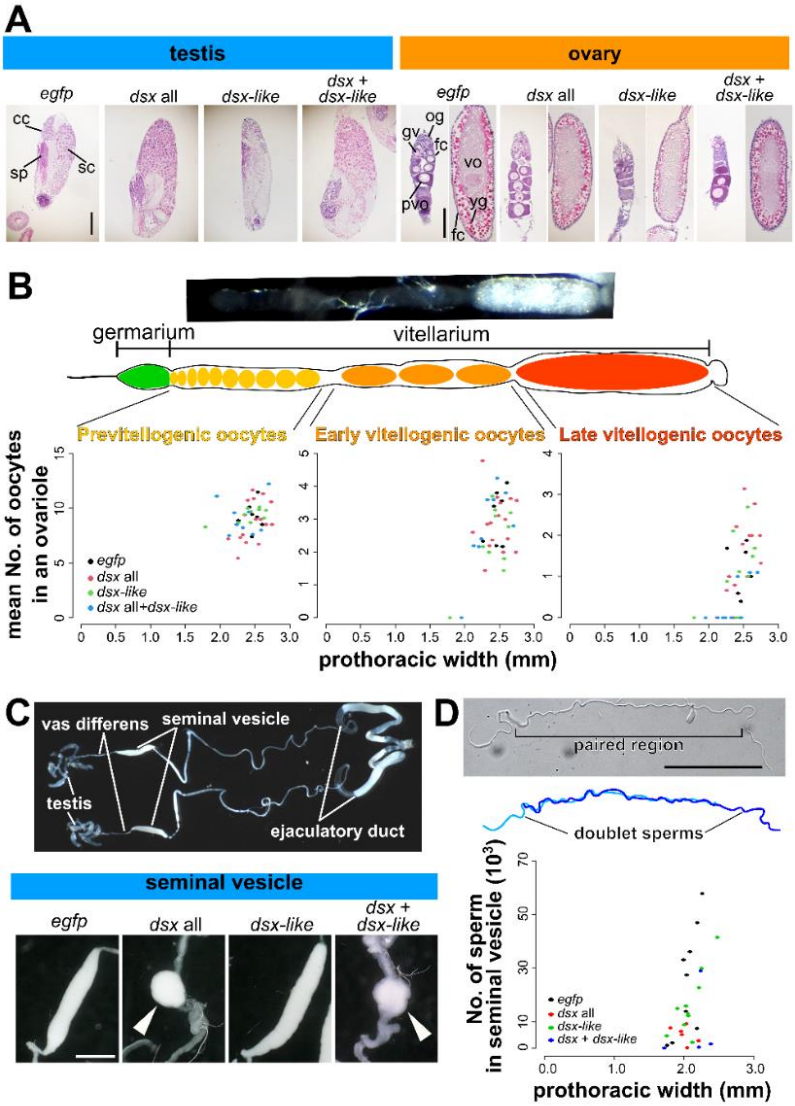

Figure 3. Function of *doublesex* in reproductive systems and fecundity. (A) Effects of *dsx* and *dsx-like* RNAi on gonad morphology and gametogenesis. In images of the ovary, the left and right panel in each treatment show germarium/previtellogenesis and vitellogenesis, respectively. cc, cystocyte; fc, follicle cell; gv, germinal vesicle; og, oogonia; pvo, previtellogenic oocyte; sc, spermatocyte; sp, sperm; yg, yolk granule; vo, vitellogenic oocyte. (B) The effect of *dsx* and *dsx-like* RNAi on oocyte number in each oogenetic stage. The upper panels are images of an ovariole in *T. domestica*. The lower panel shows scatter plots of oocyte numbers and prothoracic width. Results of the generalized linear model analysis are in Tables 4 (female) and 5 (male). (C) The effect of *dsx* and *dsx-like* RNAi on the seminal vesicle. The upper panel is a gross image of the male reproductive system. The lower one shows the phenotype of each treatment. (D) The effect of *dsx* and *dsx-like* RNAi on sperm number in seminal vesicles. The upper panels are images of sperm in *T. domestica*. The sperm of *T. domestica* is usually paired with other sperm. The lower panel shows a scatter plot of sperm numbers by prothoracic width. Scales: 50 μm (A and C); 10 μm (D). Sample size are also listed in Tables 4 (D) and 5 (C).

301 **Cryptic role of *doublesex* for female-specific transcripts in *T. domestica***

302 Previous studies in Hemimetabola (*Takahashi et al., 2021*; *Wexler et al., 2015*;
303 *Zhuo et al., 2018*), and our results in Zygentoma show that *dsx* is not essential for the
304 formation of female phenotypes in non-Holometabola. In contrast, considering the
305 fact that the *dsx* female-specific isoform retains ORFs in non-Holometabola, there is a
306 still possibility that *dsx* may have some function in non-holometabolan females. To
307 investigate this functionality, we focused on the effect of *dsx* on female-specific gene
308 expression.

309 We focused on the *vitellogenin* (*vtg*) gene, one of the major egg yolk proteins,
310 which is specifically expressed in females of Bilateria (Byrne et al., 1989; *Hayward et*
311 *al., 2010*). In the Holometabola, *dsx* promotes *vtg* mRNA expression in females and
312 represses it in males (*Shukla and Palli, 2012*; *Suzuki et al., 2003*; *Thongsaiklaing et*
313 *al., 2018*). Our RNA-seq analysis showed that levels of the three *vtg* mRNAs in *T.*
314 *domestica* were more than 10000-fold higher in females than in males (Figure 4A–C).
315 We found that the *vtg* mRNAs were expressed at 40–100-fold higher levels in *dsx*
316 RNAi males than in the control males (Figure 4D and Table 2). Notably, the *dsx*
317 RNAi females produced around half the amount of *vtg* mRNA as the controls. The
318 *dsx-like* RNAi and a double-knockdown of *dsx* and *dsx-like* also significantly reduced
319 the expression of *vtg* in females (Figure 4E and Table 2).

320 This result is the first case that *dsx* can promote female-specific *vitellogenin*
321 expression in non-holometabolan species, even though it does not affect female
322 phenotypes such as the oocyte size and number. This finding suggests that it has
323 opposite functionality between males and females in *T. domestica* at the gene-
324 regulatory level.

325

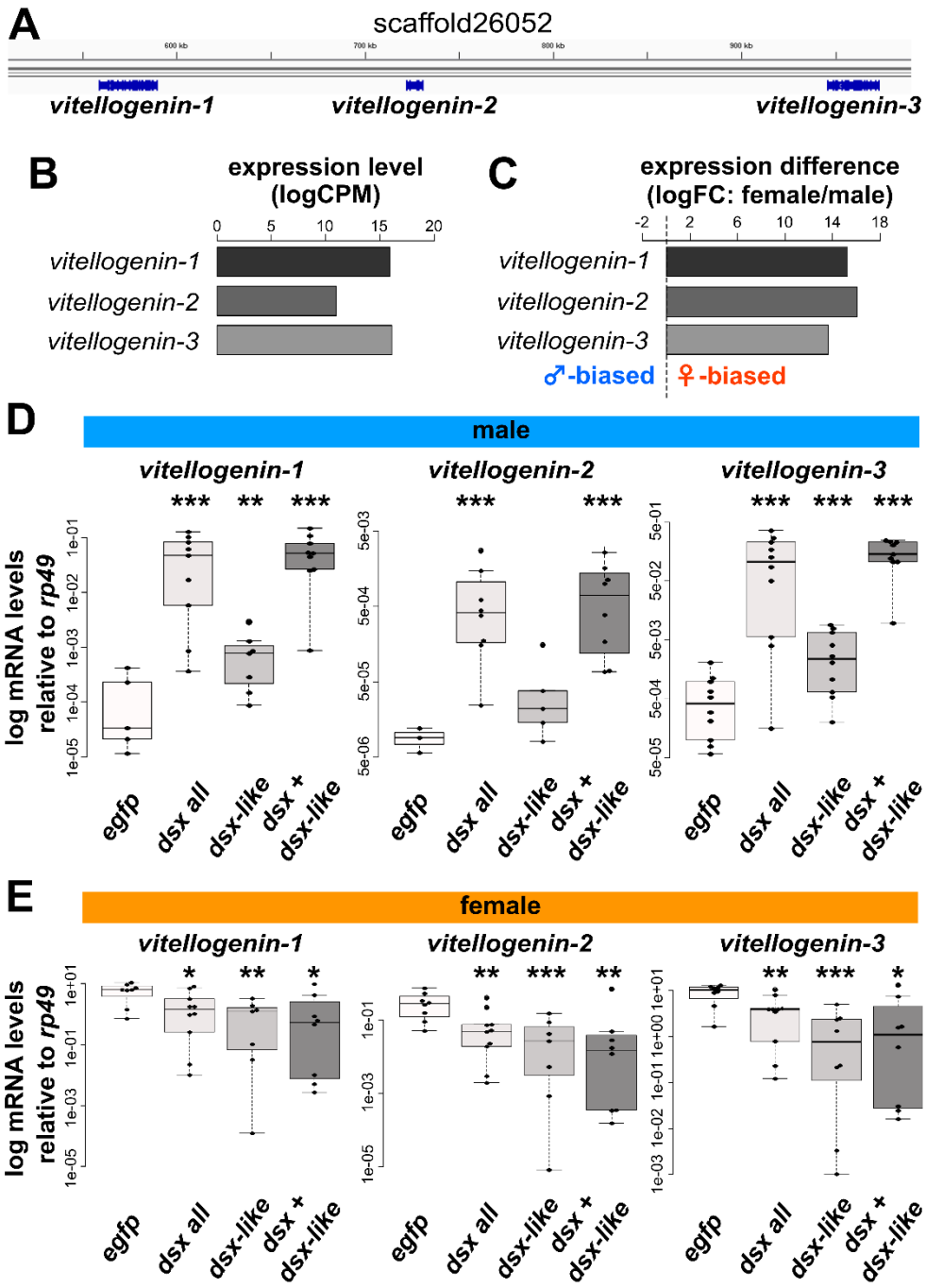

Figure 4. Function of *doublesex* in *vitellogenin* gene expression. (A to C) Features of *vitellogenin* (*vtg*) genes of *Thermobia domestica*. An image of the *vtg* gene locus in an Integrated Genome Viewer (A). The *vtg* genes are highly expressed in females (B and C). The source data of B and C are provided as Figure4–source data 1. (D and E) Effect of *dsx* and *dsx-like* RNAi on *vtg* genes' expression in males (D) and females (E). The decreases were about 2/5–1/5, 1/10–3/50, and 1/9–1/20 in *dsx*, *dsx-like*, and both the genes RNAi females. The mRNA expression levels are shown as logarithmic scales. Each plot represents an individual. Sample sizes are listed in Table 2 (C and D). Results of Brunner–Munzel tests are indicated by asterisks: **P* < 0.05; ***P* < 0.01; ****P* < 0.001 and is also described in Table 2. *P* > 0.05 is not shown.

337 **Differences of *doublesex* sequences between single- and dual-functional species**

338 Genes can gain new functions due to gene duplication, co-factor function,
339 changes in *cis*- or *trans*-region (*Carroll, 2005*; Ganfornina and Sánchez, 1999; *Mann*
340 *and Carroll, 2002*), or acquiring new exons. *dsx* paralog (*dsx-like*) found in this study
341 did not contribute to female phenotypes (Figure 2 and 3). The female and male
342 isoforms of *dsx* share the same DNA-binding domain, and *intersex*, a co-factor gene
343 of *dsx*, contributes to the formation of female traits in *Nilaparvata lugens* (*Zhang et*
344 *al., 2021*), which has the single-functional *dsx*. These facts indicate that the gene
345 duplication, neo-functionalization of co-factors, and changes in *cis*-regulatory
346 elements are not likely to contribute to the evolution of the dual-functionality. Thus,
347 we explored the remaining possibilities: novel exons or *trans*-regions.

348 We found that there are alternative splice types in *T. domestica*, which has an
349 alternative 5′ splice site, and in Pterygote insects, which have a mutually exclusive
350 exon, but did not find any differences of exon structure between species with single-
351 functionality of *dsx*, and those with dual-functionality (Figure 5A).

352 We finally discovered amino acid sequences in the female-specific region that
353 differed between taxa with single- and dual-functionality of *dsx*. *dsx* isoforms are
354 sexually different in the OD domain. This domain was divided into common, female-
355 specific, and male-specific regions. Our multiple alignment analysis revealed that the
356 female-specific region was highly conserved among the taxa with dual-functionality
357 of *dsx*, but not among those with single functionality (Figures 5B, Figure 5–figure
358 supplement 1). In contrast, the male-specific region was not highly conserved among
359 the taxa with dual-functional *dsx* (Figure 5–figure supplement 2).

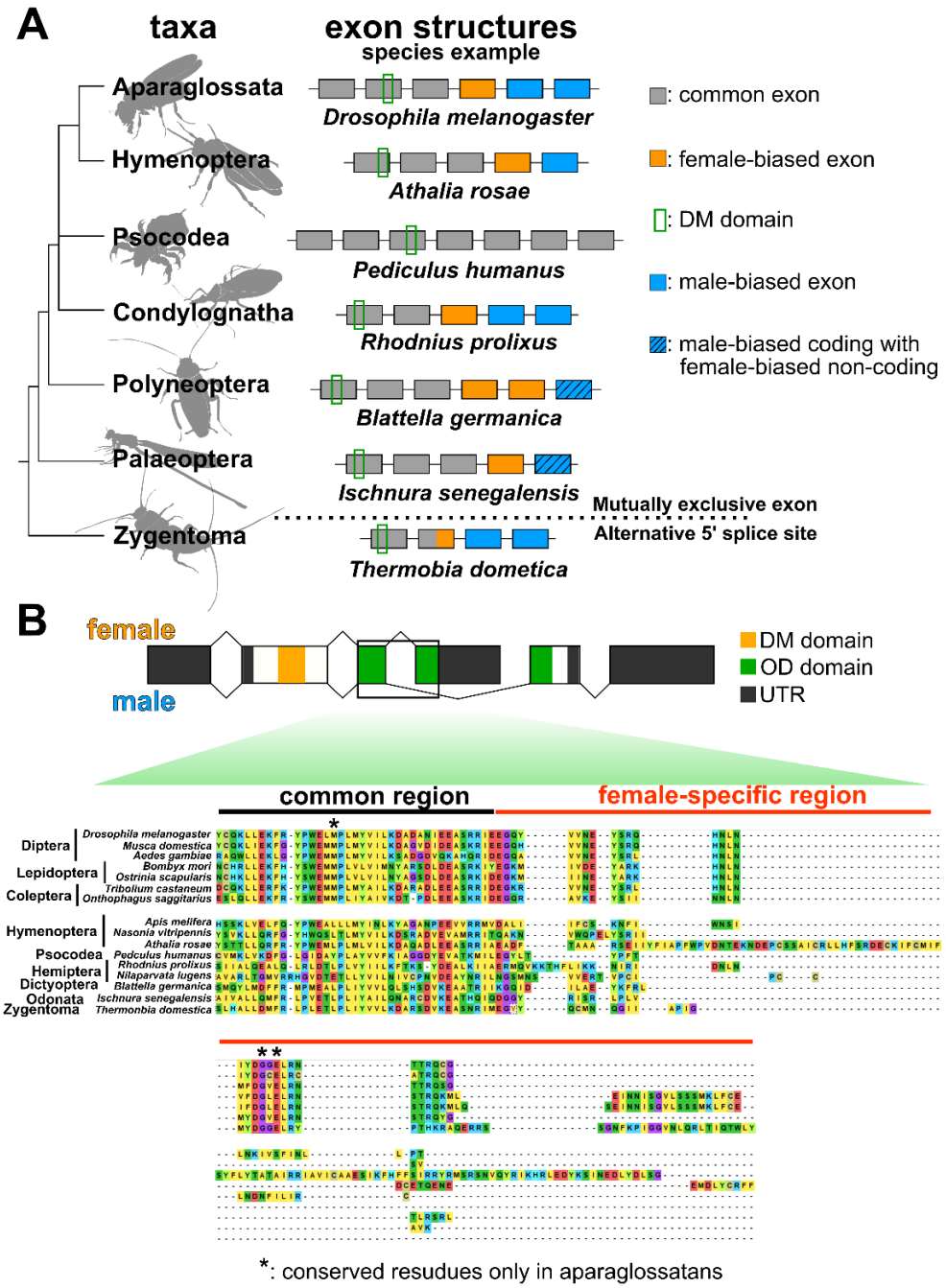

Figure 5. Comparisons of molecular features in *doublesex* among insect taxa. (A) Exon structure of *dsx* among insect taxa. The coding region of *dsx* is shown. The phylogenetic relationship is that of *Misof et al. (2014)* (B) amino acid sequence of Dsx among insect taxa. The upper image shows the *dsx* structure of *Drosophila melanogaster*. Asterisks indicate conserved residues in Aparaglossata.

Discussion

A novel type of the output in the sex differentiation system

We show that the *dsx* of *Thermobia domestica* is essential for producing male phenotypes, but does not contribute to female phenotypes. In contrast to the phenotypes, this study showed that the female-specific *vitellogenin* genes are slightly promoted by *dsx* in *T. domestica* females. These facts indicate that *dsx* in *T. domestica* has an opposite transcription-regulatory function in males and females. Therefore, in *T. domestica*, *dsx* contributes only to male differentiation at the phenotypic level, but affects both sexes at the transcription-regulatory level (seemingly useless nature).

There have been two known types of outputs of the insect sex differentiation system: one that can regulate feminization via both transcription-regulation and phenotypes, and one that cannot. The former is found in Diptera, Lepidoptera, and Coleoptera (e.g., Luo and Baker, 2015; Suzuki et al., 2003; Shukla and Palli, 2012), the latter in Dictyoptera and Hemimetabola (*Wexler et al., 2019; Zhuo et al., 2018*). In some species, such as the dung beetle *Onthophagus taurus*, *dsx* contributes only to male trait formation in some tissues (*Ledón-Rettig et al., 2017*). In these species, *dsx* is also responsible for producing traits of both sexes in other tissues. Therefore, it is likely that the former type is the primary capability of the sex differentiation systems in these species and that the function for promoting female differentiation may tissue-specifically become silent. In contrast, the seemingly useless nature of *dsx* for females in *T. domestica* is a third type of the insect sex differentiation system (Figure 6A). This third type indicates that phenotypic and transcription-regulatory levels do not necessarily coincide in the output of sex differentiation systems.

The sex differentiation systems of crustaceans, vertebrates, and nematodes have DMRT family transcription factors as bottom factors that are responsible for promoting male differentiation (*Kato et al., 2011*; *Kopp, 2012*; *Raymond et al., 1998*; *Raymond et al., 2000*). No hierarchical discrepancy has been found in the output of the sex differentiation system of these animals. Therefore, the output of the sex differentiation system in most animals can be classified into three categories: that are capable of contributing to 1) only masculinization (crustaceans, nematodes, vertebrates, Hemiptera, and Dictyoptera), 2) both masculinization and feminization (Diptera, Lepidoptera, and Coleoptera) or 3) both masculinization and feminization at the transcription-regulatory level but only masculinization at the phenotypic level (*T. domestica*).

On the origin of the sex-specific splicing of *doublesex*

In pterygote insects (e.g., *Burtis and Baker, 1989*; *Shukla and Palli, 2012*; *Mine et al., 2017*; *Ohbayashi et al., 2001*; *Takahashi et al., 2019*; *Wexler et al., 2019*; *Zhuo et al., 2018*), *dsx* has sex-specific isoforms, except for a termite *Reticulitermes speratus* (*Miyazaki et al., 2021*). In contrast, *dsx* is controlled via a male-specific transcription in chelicerates and crustaceans (*Kato et al., 2011*; Li et al., 2018; *Panara et al., 2019*; *Pomerantz et al., 2015*). Here, sex-specific splicing regulation is observed in *dsx* of *T. domestica*, suggesting that sex-specific splicing regulation originated between the common ancestor of Branchiopoda and Hexapods and the common ancestor of Dicondylia (Zygentoma + Pterygota) (Figure 6A).

On the origin of the role of the insect sex differentiation system for females

There are discrepancies in the output of the sex differentiation system in *T. domestica* at the phenotypic and transcription-regulatory levels. In such a case, it has

been proposed to map the characteristics of each hierarchical level separately on a phylogenetic tree (c.f., *Abouheif, 1999*).

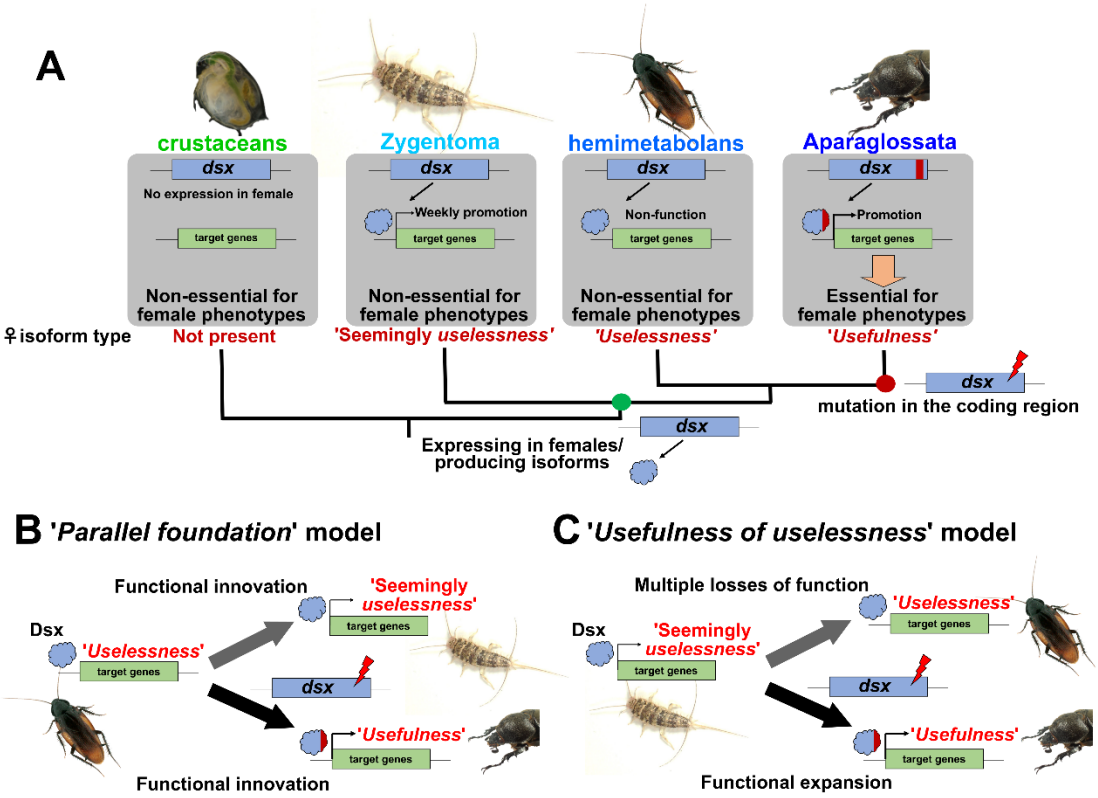

Figure 6. Evolutionary transition of outputs of the insect sex differentiation system. (A) phylogenetic mapping of functionality of *dsx* for females. crustaceans: *Kato et al. (2011)*; Zygentoma: this study; hemimetabolans: *Wexler et al. (2019), Zhuo et al. (2018);* Aparaglossata: e.g., *Shukla and Palli (2012), Suzuki et al. (2003)*. (B) '*Parallel foundation*' model. (C) '*Usefulness of useless*' model.

At the phenotypic level, previous studies have focused on taxon-specific or highly complex sex differences, leaving open the possibility of a secondary loss of function of *dsx* for females. However, the single-functionality of *dsx* even in *T. domestica*, which has an ancestral, simple sex difference, supports a single origin for *dsx* single-functionality. Based on a recent phylogenetic hypothesis (*Beutel et al., 2017*; *Misof et al., 2014*), the transition from the single- to dual-functionality is estimated to have occurred in the common ancestor of Aparaglossata (holometabolan

insects excluding Hymenoptera) (Figure 6A). At the phenotypic level, our findings ensure the evolutionary model by *Wexler et al. (2019)* that *dsx* initially acquired sex-specific isoforms and later became essential for female differentiation.

At the level of gene regulation, *dsx* in *T. domestica* can slightly promote the transcription of female-specific genes. Therefore, it is estimated that the common ancestor of Dicondylia already possessed the sexual dimorphic transcriptional control of *dsx*. In this case, it is inferred that the transcription-promoting function of female-specific genes was secondarily lost in hemimetabolan insects. Alternatively, it is possible that the common ancestor of the Dicondylia had also the single-functionality at the level of transcriptional regulation and that Zygentoma and Aparaglossata independently acquired the ability to promote transcription in females.

The question is how the function of *dsx* for the female phenotype evolved. We have found differences in the sequence of the female-specific region of *dsx* between phenotypically single-functional and dual-functional taxa. This region is located in the oligomerization (OD) domain, interacts with transcription factors (*An et al., 1995*; *Erdman et al., 1996*; *Ghosh et al., 2019*; *Romero-Pozuelo et al., 2019*) and transcriptional mediators such as *intersex* which is essential for female differentiation (*Gotoh et al., 2016*; *Morita et al., 2019*; *Xu et al., 2019*; *Yang et al., 2008*). Studies in *Blattella germanica* described low conservation of the OD domain (*Wexler et al., 2019*). *Baral et al. (2019)* also reported that the rate of non-synonymous substitutions in the female-specific region is low in Aparaglossata and high in Hymenoptera. However, the evolutionary significance of this region has been unclear. Our result suggests that the accumulation of mutations in female-specific regions has led to the female-differentiating functions at the phenotypic level (Figure 6). It was theoretically predicted that non-functional isoforms gain functions through mutation accumulation

in coding regions (*Keren et al., 2010*). The functional evolution of *dsx* in insects may fit this prediction.

Evolutionary scenarios for the transition of the output of the sex differentiation system

In conclusion, we propose two alternative scenarios for the transition of the outputs of the insect sex differentiation system.

"*Parallel foundation*" hypothesis (Figure 6B): *dsx* has independently acquired the function for promoting female transcription in Zygentoma and Aparaglossata, and also gained the entirely novel role in phenotypic differentiation in females through the accumulation of coding mutations in Aparaglossata. This is the hypothesis that a useful functionality has arisen from a completely useless functionality.

"*Usefulness of uselessness*" hypothesis (Figure 6C): *dsx*, through the accumulation of mutations in its coding region, enhanced its weak transcription-promoting ability in females and became essential for producing the female phenotypes. This is the hypothesis that a useful functionality arose from a seemingly useless functionality.

Both these hypotheses can explain the diversity in outputs of the sex differentiation system via the accumulation of coding mutations in existing genes. Thus, a heterotypic evolution may drive the evolution of outputs of the sex differentiation systems. Textbook examples of the heterotypic evolution include a mutation of human *hemoglobin β* leading to sickle cells and coding mutations of *Ultrabithorax* that resulted in suppressed leg development in insects (reviewed in *Arthur, 2010*; *Gilbert, 2013*; *Futuyma and Kirkpatrick, 2017*). So far, heterotypy at the molecular level is considered as the change in the molecular function leading to entirely novel or no functions from existing functions of the molecule in phenotypes. On the other hand, the female isoform of *dsx* shows no function in female phenotypes.

Our hypotheses are models that a non-functional isoform gains functionality at the phenotypic level. The heterotypic evolution may need to be divided into modification from existing functions and innovation from non-functionality at phenotypic level.

In this study, we succeeded in detecting the transcription-promoting ability of *dsx* in females by examining the expression of *vitellogenin*. In hemimetabolan insects. the transcription-promoting function in females has not been found in *vitellogenin* (*Wexler et al., 2019*; *Zhuo et al., 2018*), but might be detected in other female-specific genes. Future comprehensive examination of the effects of *dsx* by transcriptome and comparisons at the mega-evolutionary level, i.e., higher taxa than families (*Arthur, 2003*), using broad insect taxa will test these hypotheses.

Materials and Methods

Animals

A firebrat, *Thermobia domestica* (Packard, 1873), was used as an emerging model apterygote. *T. domestica* is one of the species belonging to the Zygentoma (Lepismatidae). The insects were kept at 37°C in total darkness condition and fed with fish food (TetraFin Goldfish Flakes, Tetra GmbH, Melle, Germany) in our laboratory. Stock colonies were reared in plastic cases of 30 cm×40 cm or 18 cm × 25 cm in length. Eggs were collected from tissue paper in the case and incubated at 37°C. For nymphal RNAi analysis, colonies of hatched nymphs were reared up to the fourth instar in a six-well plate and then transferred into 24-well plates to be kept individually. For adult RNAi analysis, adult insects were collected from the stock colony and transferred into the plates. For nymphal RNAi analysis, we used firebrats from April to June, 2019, February to April, April to July, and September to

December, 2020. For adult RNAi, adult firebrats were manipulated from June to July, 2020.

Estimation of molt timing

Estimating the molt timing of insects is essential for the analysis of developmental processes and the functions of developmental regulatory genes. The timing of Hemi- or holometabolan insects can be estimated using morphological changes such as a wing growth. However, timing is hard to estimate in apterygote insects since they have little change in their morphology during postembryonic development. *T. domestica* forms scales in the fourth instar, and changes the number and length of its styli during the fourth to ninth instar under our breeding conditions. These features can be used to estimate molt timing, but it is difficult to apply these criteria to experiments using adults or a large number of nymphs. To resolve this problem, we used leg regeneration after autotomy and time-lapse imaging to estimate the molt timing of *T. domestica*. Autotomy occurs at the joint between the trochanter and femur in *T. domestica*. An autotomized leg regenerates after one molt (*Buck and Edwards, 1990*). For nymphal RNAi analysis, we amputated a right hindleg at the autotomic rift, using tweezers, and observed whether the leg had regenerated. This test enabled us to rapidly estimate the molt timing. For adult RNAi, time-lapse imaging was used to determine the precise time of molt. We build a time-lapse imaging system with a network camera system (SANYO, Tokyo, Japan) set in an incubator at 37°C (Figure 4–figure supplement 1A). Photos of insects in the 24-well plate were taken every five minutes. We created a time-lapse movie from the photos every 12 hours using ImageJ 1.52a (https://imagej.nih.gov/ij/) and observed whether the insects molted (Figure 4–figure supplement 1B, Video 1).

De novo genome assembly

A whole genome of *T. domestica* was sequenced to analyze the exon-intron structure of *dsx*. We selected an adult female of *T. domestica* from our stock colony and removed its alimentary canal. Genomic DNA was extracted from the sample using DNeasy Blood and Tissue Kit (QIAGEN K.K., Tokyo, Japan). A paired-end library was constructed from 1 µg of the DNA using TruSeq DNA PCR-Free LT Sample Prep kits (Illumina K.K., Tokyo, Japan) following the manufacturer's instructions. The library was run on a sequencer (HiSeq 2500; Illumina K.K., Tokyo, Japan). We obtained 417 Gb of raw reads and assembled them using Platanus v1.2.4 assembler (*Kajitani et al., 2014*) after removal of the adapter sequences.

Transcriptome analysis

To search for *doublesex* (*dsx*) and *vitellogenin* (*vtg*) homologs, we performed RNA-seq analysis. Adults of 15 ♀♀ and 15 ♂♂ of *T. domestica* were sampled 1440 minutes after a molt in December, 2019. The fat bodies of the individuals were removed using tweezers in a phosphated buffered saline (PBS; pH=7.2). Three adults were used per sample. Total RNA was extracted from 10 samples (5♀♀, 5♂♂) using RNeasy Micro kits (QIAGEN K.K., Tokyo, Japan) following the manufacturer's instructions. The concentration of purified RNA was measured using a Qubit 4 fluorometer (QIAGEN K.K., Tokyo, Japan) with Qubit RNA BR Assay kits (QIAGEN K.K., Tokyo, Japan). Paired-end libraries were constructed from 100 ng of the total RNAs using TruSeq RNA Library Prep kits v2 (Illumina K.K., Tokyo, Japan) following the manufacturer's instructions. The libraries were run on a sequence (Hiseq, Illumina, Tokyo, Japan). The library preparation and sequencing were performed by Genewiz Strand-Specific RNA-seq service. We mapped the reads obtained to the assembled genome using the HISAT2 program (Kim et al., 2019) with a default option and counted the mapped reads using the STRINGTie program

(Pertea, 2015) with default parameter settings. Differential expression gene analysis was performed based on the count matrix using the "edgeR" package *(Robinson et al., 2010*) in R-v4.0.3 (*R Core Team, 2020*). Information about the samples can be obtained from the National Center for Biotechnology Information (NCBI) BioSample database (Accession number: SAMN18175012–SAMN18175021).

Molecular phylogenetic analysis

Dsx is a member of the Doublesex and Mab-3 Related transcriptional factors (DMRT) family, and has a DNA binding domain, Doublesex and Mab-3 (DM) domain. Pancrustacea generally has four DMRT family genes, Dsx, Dmrt11, Dmrt93B, and Dmrt99B (*Mawaribuchi et al., 2019*). Phylogenetic analysis of Dsx homologs was performed using the amino acid sequences of the DM domain. We used the Dsx sequences of *D. melanogaster* as a query and obtained 97 metazoan DMRT family proteins from the NCBI and the i5k databases (https://i5k.nal.usda.gov/) and our genome data of *T. domestica* by the BLAST analysis (listed in Table 1). We then aligned the sequences using MAFFT version 7 (*Katoh et al., 2013*) with the -linsi option (to use an accuracy option, L-INS-i) and manually extracted the DM domain, which consisted of 61 amino acids (Figure 1–figure supplement 1). Molecular phylogenetic analysis of the aligned sequences was performed using a maximum likelihood method after selecting a substitution model (JTT matrix-based model) with MEGA X (*Kumar et al., 2018*). Bootstrap values were calculated after 1000 replications.

Full-length cDNA and exon-intron structures

To elucidate the exon-intron structures of Dsx and Dsx-like, we determined the full-length cDNA sequences using a Rapid Amplification of cDNA Ends (RACE) method and performed a BLAST analysis for our genome database of *T. domestica*.

We extracted total RNA from eggs, whole bodies, fat body, and gonads of nymphs and adult females and males of *T. domestica* using TRI Reagent (Molecular Research Center Inc., Ohio, USA) following the manufacturer's instructions. The total RNAs were treated with RNase-Free DNase I (New England BioLabs Japan Inc., Tokyo, Japan) to exclude remaining genomic DNA and purified by phenol/chloroform extraction and ethanol precipitation. For 5′ -RACE analysis, mRNAs were purified from 75 μg of the total RNAs using Dynabeads mRNA Purification kit (Thermo Fisher Scientific K.K., Tokyo, Japan) following the manufacturer's instruction. We then ligated an RNA oligo at the 5'-end of the mRNA using GeneRacer Advanced RACE kits (Thermo Fisher Scientific K.K., Tokyo, Japan). For 3′-RACE analysis, we ligated an RNA oligo of the SMART RACE cDNA Amplification Kit (Takara Bio Inc., Shiga, Japan) at 3′-end of the total RNA during reverse transcription. First stranded (fs-) cDNA was generated from the RNAs using SuperScript III Reverse Transcriptase (Thermo Fisher Scientific K.K., Tokyo, Japan). We used primers specific to the RNA oligos and performed RACE analysis by nested RT-PCR using Q5 High-Fidelity DNA polymerase (New England BioLabs Japan Inc., Tokyo, Japan). The primers specific to *dsx* and *dsx-like* were made from sequences of the relevant genomic regions and are listed in Table 6. The amplicons were separated using the agarose gel-electrophoresis and cloned using TOPO TA Cloning Kit for Sequencing (Thermo Fisher Scientific K.K., Tokyo, Japan) following the manufacture's protocol. We used a DH5α *Escherichia coli* strain (TOYOBO CO., LTD., Osaka, Japan) as the host cell. Plasmids were extracted using the alkaline lysis and purified by phenol-chloroform and ethanol precipitation. The nucleotide sequences of the cloned amplicons were determined from the purified plasmids by the Sanger Sequencing service of FASMAC Co. Ltd. (Kanagawa, Japan). We then

605 searched the genomic region of the full-length cDNA sequences of *dsx* and *dsx-like*
606 via local blastn analysis.

607 **Reverse transcription-quantitative PCR (RT-qPCR)**

608 To quantitative mRNA expression levels, we performed RT-qPCR analysis.
609 For investigating the sex-specific expression profile of *dsx* and *dsx-like*, we used the
610 fat body of adults of *T. domestica* since the sexes can be distinguishable by the
611 external morphology at this stage. Fat bodies also exhibit sex-specific physiological
612 functions in adults. Thirteenth instar individuals and adults after molting were
613 sampled for nymphal and adult RNAi analyses, respectively. The sample sizes are
614 reported in the Table 2. We dissected the individuals in PBS and collected their fat
615 body in 2 ml tubes containing TRI Reagent (Molecular Research Center Inc., Ohio,
616 USA). The fat bodies then were disrupted using a TissueLyser LT small beads mill
617 (QIAGEN K.K., Tokyo, Japan). These disrupted samples were preserved at −80°C
618 until used. Total RNA was extracted from the samples according to the manufacture's
619 protocol for the TRI Reagent. Extracted RNA was treated with 2% RNase-free DNase
620 I (New England BioLabs Japan Inc., Tokyo, Japan) at 37°C for 40 minutes and
621 purified by phenol/chloroform extraction and ethanol precipitation. We measured the
622 concentration of the total RNA using a spectrophotometer (DS-11+, Denovix Inc.,
623 Wilmington, USA). fs-cDNA was synthesized from 350 ng of the total RNA using
624 SuperScript III Reverse Transcriptase (Thermo Fisher Scientific K.K., Tokyo, Japan).
625 We diluted the fs-cDNA to 1:2 with MilliQ water and preserved it at −30°C until it
626 was used in RT-qPCR assay. The RT-qPCR assays were performed using a
627 LightCycler 96 instrument (Roche, Basel, Switzerland) according to the
628 manufacture's protocol with the THUNDERBIRD SYBR qPCR Mix (TOYOBO Co.
629 Ltd., Osaka, Japan). The reaction volume was 10 µl. We used 1 µl of the fs-cDNA as

630 templates. The preparation of the RT-qPCR solution proceeded on ice. The protocol
631 of the RT-qPCR was as follows: preincubation at 95°C for 600 seconds and 45 cycles
632 of three-step reactions, such as denaturation at 95°C for 15 seconds, annealing at 60°C
633 for 15 seconds and extension at 72°C for 45 seconds. We used *ribosomal protein 49*
634 (*rp49*) as a reference gene, as described by *Ohde et al. (2011)*. We designed primer
635 sets of the target genes by the Primer3Web version 4.1.0 (*Untergasser et al., 2012*)
636 following the manufacture's recommended condition of the THUNDERBIRD SYBR
637 qPCR Mix. We confirmed the primers' specificity using melting curves ranging from
638 65°C to 95°C. We selected primer sets exhibiting a single peak. The primers are listed
639 in Table 6. Each RT-qPCR was technically replicated three times. Some samples were
640 excluded before analyzing the data when the Ct value of any genes was not detected
641 (ND) in one or more replicates or when the Ct value of the reference gene deviated
642 from that of other samples. In these removed data, a technical error was suspected.
643 We calculated the expression level of target genes by the $2^{-\Delta\Delta Ct}$ method (*Livak and*
644 *Schmittgen, 2001*) and performed the Brunner–Munzel (BM) test for ΔCt value. The
645 BM test was carried out using R-v4.0.3. with the *brunnermuzel.test* function of the
646 "brunnermuzel" package (https://cran.r-
647 project.org/web/packages/brunnermunzel/index.html). Holm's method was used for
648 multiple comparison analyses between the control and treatments. The data are listed
649 in Table 2. Also, its source data can be found in Table2–Source Data 1. In the *dsx*
650 expression of the RNAi male, we performed the Smirnov-Grubbs (SG) test for ΔCt
651 value using the *grubbs.test* function of the "outliers" package in R (https://cran.r-
652 project.org/web/packages/outliers/index.html) (Table 3). An outlier was detected in
653 the *dsx* RNAi male. We repeatedly performed the SG test using the data excluding the

outlier. No further outliers were detected. Lastly, we re-analyzed the data, excluding the outlier, using the BM test (Table 2).

RNAi analysis

Nymphal RNAi can be used to analyze the roles of genes during postembryonic development. The sexual differentiation of insects is generally assumed to be a cell-autonomous mechanism that is independent of systemic hormonal- control (*Verhulst and van de Zande, 2015*) as discussed in *De Loof and Huybrechts (1998)* and *Bear and Monteiro (2013)* and progresses during postembryonic development. Therefore, nymphal RNAi is the most effective tool to investigate the roles of genes on sexual trait formation. To reduce the possibility of off-target effects, the dsRNA was designed to avoid the region of the DM domain. We also confirmed that the dsRNA had no contiguous matches of more than 20 bases with other regions of the genome. To produce templates for the dsRNA, we cloned the regions of *dsx* and *dsx-like* from the fs-cDNA using the same method as the RACE analysis. We amplified the template DNAs from purified plasmids with PCR using Q5 High-Fidelity DNA Polymerase and purified the amplified DNA with the phenol/chloroform extraction and the ethanol precipitation. dsRNA was synthesized from the purified DNA using Ampliscribe T7-Flash Transcription kits (Epicentre Technologies, Co., Wisconsin, USA). We designed the PCR primers using the Primer3Web version 4.1.0 (*Untergasser et al., 2012*). The PCR primers are listed in Table 6. In nymphal RNAi analysis, we injected the dsRNAs repeatedly into the abdomen of the nymphs of *T. domestica* with each molt from the fourth or fifth instar to thirteenth instar to sustain the RNAi effect during postembryonic development. The initial stage was the same within a single experiment. This repeated nymphal RNAi was effective in some insects such as *Blattella germanica* (*Wexler et al., 2014*). We

679 sampled the individuals one, three, and five days after molting, using phenotypic
680 observations, analysis of *dsx* knockdown effects, and the oocyte size and number. To
681 determine the sex of individuals, we initially observed the gonads: testis and ovary. In
682 our nymphal RNAi analysis, the gonads completely formed and there was no
683 difference between the control and *dsx* RNAi individuals in external morphology
684 (Figures 1–figure supplement 3, Figure2–figure supplement 1A). Therefore, at least in
685 this assay, the gonad morphology was effective for the identification of the sex of *dsx*
686 RNAi individuals. Individuals with testis were males and those with ovaries were
687 females. For the analysis of *vtg* genes, we used the adult RNAi assay. *T. domestica*
688 molts throughout its life, even after sexual maturation, and produces *vtg* during each
689 adult instar (*Rouset and Bitsch, 1993*). In the adult RNAi analysis, we injected dsRNA
690 repeatedly into the adults every three days. The dsRNA was initially injected into
691 adults 12 hours after molting. We sampled the adults at 720±20 minutes after
692 subsequently molts, to analyze the *vtg* mRNA levels.

693 **Phenotype observation**

694 We dissected thirteenth instar individuals in PBS using tweezers and removed
695 the thoraxes, reproductive systems, and external genital organs. We took images using
696 the digital microscope system (VHX-5000, KEYENCE, Tokyo, Japan). The thoraxes
697 and external genital organs were fixed with FAA fixative (formaldehyde: ethanol:
698 acetic acid = 15:5:1) at 25°C overnight and then preserved in 90% ethanol. We used
699 the length of the prothorax as an indicator of body size. To measure the prothoracic
700 width, the prothoracic notum was removed from the fixed thorax after treatment with
701 10% NaOH solution at 60°C for 30 minutes to dissolve the soft tissues. The notum
702 was mounted in Lemosol on a microscope slide. The prepared specimens were imaged
703 using a KEYENCE VHX-5000. With the microscope at 50×, the length of the notum

was measured. The ovipositor length and oocyte size were also measured using the microscope at 20× and 50×. The oocyte size was taken to be the major length of the late vitellogenic oocyte at the posterior most part of the ovariole. To count the sperm number, sperm was collected from seminal vesicles and diluted with 5 ml MilliQ water. 50 µl of the diluted sperm was spotted on a microscope slide and dried overnight. We technically replicated the measurement three times for ovipositor length and six times in sperm number and calculated these means. Measurement was performed by blinding the treatment. We counted the number of oocytes in ovarioles using an optical microscope at 50× (Olympus, Tokyo, Japan). A generalized linear model (GLM) was used to analyze differences in ovipositor length and oocyte size (length data) and sperm and oocyte number (count data) among RNAi treatments. The body size, target genes, and interactions between the target genes were used as explanatory variables. The length was assumed to follow a Gaussian distribution, and the count data to have a negative binomial distribution. We used R-v4.0.3 in these analyses and the *glm* and the *glm.nb* (MASS package) functions for the length and count data, respectively. To analyze the contribution of the explanatory variables, a likelihood ratio test for the result of GLM was performed using the *Anova* function of the car package. The statistical results are listed in Tables 4 (female) and 5 (male). Also, the source data are reported in Table 4–source data 1 and Table 5–source data 1.

Scanning Electron Microscopy (SEM)

The NanoSuit method (*Takaku et al., 2013*) was used for the SEM analysis. Male penises and female ovipositors preserved in 90% ethanol were washed with distilled water and immersed in 1% Tween20 at 25°C for 10 minutes. The samples were mounted on stubs and imaged using a low-vacuum SEM (DX-500; KEYENCE, Tokyo, Japan).

729 **Histology**

730 The gonads of RNAi individuals were fixed with Bouin's fixative (saturated picric
731 acid: formaldehyde: glacial acetic acid = 15:5:1) at 25°C overnight and washed with
732 90% ethanol plus Lithium Carbonate (Li_2CO_3). The ovipositors of RNAi individuals
733 were fixed with FAA fixative at 25°C overnight and then were transferred into 90%
734 ethanol. The samples were dehydrated and cleared with an ethanol-butanol series. The
735 cleared samples were immersed and embedded in paraffin at 60°C. The paraffin
736 blocks were polymerized at 4°C and cut into 5 µm thick sections using a microtome
737 (RM2155: Leica, Wetzlar, Germany). The sections were mounted on microscope
738 slides coated with egg white-glycerin and stained using Delafield's Hematoxylin and
739 Eosin staining. The stained slides were enclosed with Canada balsam. We observed
740 the slides on an optical microscope (Olympus, Tokyo, Japan) and took photos using a
741 digital single-lens reflex camera (Nikon, Tokyo, Japan).

742 **Comparison of exon-intron structure and amino acid sequences**

743 We obtained exon-intron structures of *dsx* in seven insect species from NCBI. The
744 female- and male-specific regions were visualized as red and blue colors, respectively.
745 The exon-intron structures were mapped on a phylogenetic hypothesis based on *Misof*
746 *et al. (2014)*. We obtained amino acid sequences of Dsx isoforms of 10 species from
747 the NCBI database. *Wexler et al. (2014)* showed that *dsx* of *Pediculus humanus*
748 (Psocodea) has isoforms without sex-specificity. In this study, based on the blast
749 search and exon structure, we determined that PhDsx1 in *Wexler et al. (2019)*
750 corresponded to the *dsx* female-type and PhDsx2 to *dsx* male-type. The sequences
751 were aligned using MAFFT version 7 with a -linsi option.

752 **Data availability**

753 The draft genome data was deposited in the DNA Data Bank of Japan (Accession
754 number: DRA005797; Bioproject: PRJDB5781). The raw read data of the
755 transcriptome was in the NCBI Sequence Read Archive (Accession numbers:
756 SRR13870115–SRR13870124; Bioproject: PRJNA707122). The sequences of *dsx*
757 male-type, *dsx* female-type, and *dsx-like* are also in GenBank (Accession numbers:
758 MW711323, MW711324, and MW711325, respectively).
759

760 Acknowledgments

761 We would like to thank Dr. Takahiro Ohde (National Institute for Basic Biology;
762 Kyoto University) for his help to extract genomic DNA of *T. domestica* and for a
763 great advice to the discussion. We are also grateful to Dr. Toshiya Ando, Dr. Taro
764 Nakamura, Dr. Shinichi Morita, Dr. Hiroki Sakai, and Dr. Tatsuro Konagaya
765 (National Institute for Basic Biology) for technical advice and discussion on this
766 manuscript. We also express our gratitude to Dr. Morita for providing a photo of
767 *Daphnia magna*. Computations were performed on the NIG supercomputer at ROIS,
768 National Institute of Genetics and the Data Integration and Analysis Facility, National
769 Institute for Basic Biology. We thank the Model Plant Research Facility, NIBB
770 Bioresource Center for providing the network camera system. This work was
771 supported by the JSPS KAKENHI Grant numbers JP25660265, JP16H02596, and
772 JP16H06279 (PAGS) for TN and the Sasakawa Scientific Research Grant from The
773 Japan Science Society for YC.
774

775 Author Contributions:

YC and TN conceived this study. YC performed the cloning of *dsx* and *dsx-like*, the RNAi, the RNA-seq, and the molecular phylogenetic analysis. AT sequenced the genome. MO and TI performed the de novo genome assembly. YC and T. wrote this manuscript; all authors commented on the manuscript.

Competing Interest Statement

The authors declare that have no competing interests.

References

Abouheif E. 1999. A method for testing the assumption of phylogenetic independence in comparative data. *Evolutionary Ecology Research* **1:** 895–909.

An W, Wensink PC. 1995. Integrating sex-and tissue-specific regulation within a single *Drosophila* enhancer. *Genes & Development* **9:** 256–266.

Arthur W. 2003. Micro-, Macro-, and Megaevolution In: Hall BK, Olson WM (Eds). *Keywords and Concepts in Evolutionary Developmental Biology*. Cambridge: Harvard University Press. p. 249–260.

Arthur W. 2010. *Evolution: A Developmental Approach*. New York: John Wiley & Sons.

Bachtrog D, Mank JE, Peichel CL, Kirkpatrick M, Otto SP, Ashman TL, Hahn MW, Kitano J, Mayrose I, Ming R, Perrin N, Ross L, Valenzuela N, Vamosi JC, Tree of Sex Consortium. 2014. Sex determination: why so many ways of doing it? *PLoS Biol* **12**: e1001899.

798 Baral S, Arumugam G, Deshmukh R, Kunte K. 2019. Genetic architecture and sex–
799 specific selection govern modular, male–biased evolution of *doublesex*. *Science*
800 *Advances* **5:** eaau3753.
801 Bear A, Monteiro A. 2013. Both cell-autonomous mechanisms and hormones
802 contribute to sexual development in vertebrates and insects. *Bioessays* **35:** 725–
803 732.
804 Beukeboom LW, Perrin N. 2014. *The evolution of sex determination*. Oxford: Oxford
805 University Press.
806 Beutel RG, Yavorskaya MI, Mashimo Y, Fukui M, Meusemann K. 2017. The
807 phylogeny of Hexapoda (Arthropoda) and the evolution of megadiversity.
808 *Proceedings of the Arthropodan Embryological Society of Japan* **51:** 1–15.
809 Bopp D, Saccone G, Beye M. 2014. Sex determination in insects: variations on a
810 common theme. *Sexual Devevelopment* **8:** 20–28.
811 Boudinot BE. 2018. A general theory of genital homologies for the Hexapoda
812 (Pancrustacea) derived from skeletomuscular correspondences, with emphasis on
813 the Endopterygota. *Arthropod Structure & Development* **47:** 563–613.
814 Buck C, Edwards JS. 1990. The effect of appendage and scale loss on instar duration
815 in adult firebrats, *Thermobia domestica* (Thysanura). *Journal of Experimental*
816 *Biology* **151:** 341−347.
817 Burtis KC, Baker BS. 1989. *Drosophila doublesex* gene controls somatic sexual
818 differentiation by producing alternatively spliced mRNAs encoding related sex–
819 specific polypeptides. *Cell* **56:** 997–1010.
820 Byrne BM, Gruber MABG, Ab G. 1989. The evolution of egg yolk proteins. *Progress*
821 *in Biophysics &Molecular Biology* **53:** 33–69.

822 Caroll SB. 2005. Evolution at Two Levels: On Genes and Form. *PLoS Biol.* **3,:**e245.

823 Chandler JC, Fitzgibbon QP, Smith G, Elizur A, Ventura T. 2017. *Y-linked iDmrt1*

824 paralogue (*iDMY*) in the Eastern spiny lobster, *Sagmariasus verreaux*i: The first

825 invertebrate sex-linked *Dmrt*. *Developmental Biology* **430**: 337–345.

826 Darwin C. 1871. *The Descent of Man, and Selection in Relation to Sex vol. 1* London:

827 John Murray.

828 De Loof A, Huybrechts R. 1998. "Insects do not have sex hormones": a myth?

829 *General and Comparative Endocrinology* 111: 245–260.

830 Emeljanov AF. 2014. The evolutionary role and fate of the primary ovipositor in

831 insects. *Entomological Review* **94:** 367–396.

832 Erdman SE, Chen HJ, Burtis KC. 1996. Functional and genetic characterization of the

833 oligomerization and DNA binding properties of the *Drosophila doublesex* proteins.

834 *Genetics* **144:** 1639–1652.

835 Fryxell DC, Weiler DE, Kinnison MT, Palkovacs EP. 2019. Eco–evolutionary

836 dynamics of sexual dimorphism. *Trends in Ecology and Evolution* **34:** 591–594.

837 Futuyma D, Kirkpatrick M. 2017. *Evolution 4th edition* Sunderland: Sinauer

838 Associates.

839 Ganfornina MD, Sánchez D. 1999. Generation of evolutionary novelty by functional

840 shift. *Bioessays* **21:** 432–439.

841 Geddes P, Thomson JA. 1889. *The evolution of sex*. London: Walter Scott.

842 Gempe T, Hasselmann M, Schiøtt M, Hause G, Otte M, Beye M. 2009. Sex

843 determination in honeybees: two separate mechanisms induce and maintain the

844 female pathway. *PLoS Biol.* **7:** e1000222.

845 Ghosh N, Bakshi A, Khandelwal R, Rajan SG, Joshi R. 2019. The Hox gene
846 *Abdominal-B* uses Doublesex^{F} as a cofactor to promote neuroblast apoptosis in the
847 *Drosophila* central nervous system. *Development* **146:** dev175158.
848 Gilbert SF. 2013. *Developmental Biology 10th edition*. Sunderland: Sinauer
849 Associates.
850 Gotoh H, Zinna RA, Warren I, DeNieu M, Niimi T, Dworkin I, Emlen DJ, Miura T,
851 Lavine LC. 2016. Identification and functional analyses of sex determination genes
852 in the sexually dimorphic stag beetle *Cyclommatus metallifer*. *BMC Genomics* **17:**
853 250.
854 Gubbay J, Collignon J, Koopman P, Capel B, Economou A, Münsterberg A, Vivian
855 N, Goodfellow P, Lovell-Badge R. 1990. A gene mapping to the sex-determining
856 region of the mouse Y chromosome is a member of a novel family of
857 embryonically expressed genes. *Nature* **346:** 245–250.
858 Hasselmann M, Gempe T, Schiøtt M, Nunes-Silva CG, Otte M, Beye M. 2008.
859 Evidence for the evolutionary nascence of a novel sex determination pathway in
860 honeybees. *Nature* **454:** 519–522.
861 Hattori, Y. Murai, M. Oura, S. Masuda, S. K. Majhi, T. Sakamoto, J. I. Hattori RS,
862 Murai Y, Oura M, Masuda S, Majhi SK, Sakamoto T, Fernandino JI, Somoza GM,
863 Yokota M, Strüssmann CA. 2012. A Y-linked anti-Müllerian hormone duplication
864 takes over a critical role in sex determination. *PNAS* **109**: 2955–2959.
865 Hayward A, Takahashi T, Bendena WG, Tobe SS, Hui JH. 2010. Comparative
866 genomic and phylogenetic analysis of vitellogenin and other large lipid transfer
867 proteins in metazoans. *FEBS Letters* **584:** 1273–1278.

868 Herpin A, Schartl M. 2015. Plasticity of gene-regulatory networks controlling sex
869 determination: of masters, slaves, usual suspects, newcomers, and usurpators.
870 *EMBO Reports* **16:** 1260–1274.
871 Hildreth PE. 1965. Doublesex, a recessive gene that transforms both males and
872 females of *Drosophila* into intersexes. *Genetics* **51:** 659–678.
873 Hopkins BR, Kopp A. 2021. Evolution of sexual development and sexual dimorphism
874 in insects. *Current Opinion in Genetics & Development* **69:** 129–139.
875 Ito Y, Harigai A, Nakata M, Hosoya T, Araya K, Oba Y, Ito A, Ohde T, Yaginuma T,
876 Niimi T. 2013. The role of *doublesex* in the evolution of exaggerated horns in the
877 Japanese rhinoceros beetle. *EMBO Reports* **14:** 561–567.
878 Luo SD, Baker BS. 2015. Constraints on the evolution of a *doublesex* target gene
879 arising from *doublesex*'s pleiotropic deployment. *PNAS* **112:** 852–861.
880 Kamiya T, Kai W, Tasumi S, Oka A, Matsunaga T, Mizuno N, Fujita M, Suetake H,
881 Suzuki S, Hosoya S, Tohari S, Brenner S, Miyadai T, Venkatesh B, Suzuki Y,
882 Kikuchi K. 2012. A trans-species missense SNP in *Amhr2* is associated with sex
883 determination in the tiger pufferfish, *Takifugu rubripes* (fugu). *PLoS Genet*ics **8:**
884 e1002798.
885 Kajitani R, Toshimoto K, Noguchi H, Toyoda A, Ogura Y, Okuno M, Yabana M,
886 Harada M, Nagayasu E, Maruyama H, Kohara Y, Fujiyama A, Hayashi T, Itoh T.
887 2014. Efficient de novo assembly of highly heterozygous genomes from whole-
888 genome shotgun short reads. *Genome Reserach* **24:**1384–95.
889 Kato Y, Kobayashi K, Watanabe H, Iguchi T. 2011. Environmental sex determination
890 in the branchiopod crustacean *Daphnia magna*: deep conservation of a *Doublesex*
891 gene in the sex-determining pathway. *PLOS Genet.* **7:** e1001345.

892 Katoh K, Standley DM. 2013. MAFFT multiple sequence alignment software version
893 7: improvements in performance and usability. *Molecular Biology and Evolution*
894 **30:** 772–780.
895 Keren H, Lev-Maor G, Ast G. 2010. Alternative splicing and evolution:
896 diversification, exon definition and function. *Nature Review Genetics* **11:** 345–355.
897 Kijimoto T, Moczek AP, Andrews J. 2012. Diversification of *doublesex* function
898 underlies morph-, sex-, and species-specific development of beetle horns. *PNAS*
899 **109:** 20526–20531.
900 Kim D, Paggi JM, Park C, Bennett C, Salzberg SL. 2019. Graph-based genome
901 alignment and genotyping with HISAT2 and HISAT–genotype. *Nature*
902 *Biotechnology* **37:** 907–915.
903 Koopman P, Gubbay J, Vivian N, Goodfellow P, Lovell-Badge R. 1991. Male
904 development of chromosomally female mice transgenic for *Sry*. *Nature* **351:** 117–
905 121.
906 Kopp A. 2012. *Dmrt* genes in the development and evolution of sexual dimorphism.
907 *Trends in Genetics* **28:** 175–184.
908 Kristensen NP. 1975. The phylogeny of hexapod "orders". A critical review of recent
909 accounts. *Journal of Zoological Systematics and Evolutionary Research* **13:** 1–44.
910 Kumar S, Stecher G, Li M, Knyaz C, Tamura K. 2018. MEGA X: molecular
911 evolutionary genetics analysis across computing platforms. *Molecular Biology and*
912 *Evolution* **35:** 1547–1549.
913 Ledón-Rettig C, Zattara E, Moczek A. 2017. Asymmetric interactions between
914 *doublesex* and tissue- and sex-specific target genes mediate sexual dimorphism in
915 beetles. *Nature Communications* **8:** 14593.

916 Li S, Li F, Yu K, Xiang J. 2018. Identification and characterization of a *doublesex*
917 gene which regulates the expression of insulin-like androgenic gland hormone in
918 *Fenneropenaeus chinensis*. *Gene* **649:** 1–7.
919 Livak KJ, Schmittgen TD. 2001. Analysis of relative gene expression data using real–
920 time quantitative PCR and the $2^{-\Delta\Delta CT}$ method. *Methods* **25:** 402–408.
921 Mann RM, Caroll SB. 2002. Molecular mechanisms of selector gene function and
922 evolution. *Current Opinion in Genetics & Development* **5:** 592–600.
923 Matsuda M, Nagahama Y, Shinomiya A, Sato T, Matsuda C, Kobayashi T, Morrey
924 CE, Shibata N, Asakawa S, Shimizu N, Hori H, Hamaguchi S, Sakaizumi M. 2002.
925 DMY is a Y-specific DM-domain gene required for male development in the
926 medaka fish. *Nature* **417:** 559–563.
927 Matsuda R.1976. *Morphology and Evolution of the Insect Abdomen: With Special*
928 *Reference to Developmental Patterns and their Bearings upon Systematics.*
929 Oxford: Pergamon Press.
930 Mawaribuchi S, Ito Y, Ito M. 2019. Independent evolution for sex determination and
931 differentiation in the DMRT family in animals. *Biology Open* **8:** bio041962.
932 McQueen E, Rebeiz M. 2020. On the specificity of gene regulatory networks: How
933 does network co-option affect subsequent evolution? *Current Topics in*
934 *Developmental Biology* **139:** 375–405.
935 Mine S, Sumitani M, Aoki F, Hatakeyama M, Suzuki MG. 2017. Identification and
936 functional characterization of the sex-determining gene *doublesex* in the sawfly,
937 *Athalia rosae* (Hymenoptera: Tenthredinidae). *Applied Entomology and Zoology*
938 **52:** 497–509.
939 Misof B, Liu S, Meusemann K, Peters RS, Donath A, Mayer C, Frandsen PB, Ware J,
940 Flouri T, Beutel RG, Niehuis O, Petersen M, Izquierdo-Carrasco F, Wappler T,

941 Rust J, Aberer AJ, Aspöck U, Aspöck H, Bartel D, Blanke A, Berger S, Böhm A,
942 Buckley TR, Calcott B, Chen J, Friedrich F, Fukui M, Fujita M, Greve C, Grobe P,
943 Gu S, Huang Y, Jermiin LS, Kawahara AY, Krogmann L, Kubiak M, Lanfear R,
944 Letsch H, Li Y, Li Z, Li J, Lu H, Machida R, Mashimo Y, Kapli P, McKenna DD,
945 Meng G, Nakagaki Y, Navarrete-Heredia JL, Ott M, Ou Y, Pass G, Podsiadlowski
946 L, Pohl H, von Reumont BM, Schütte K, Sekiya K, Shimizu S, Slipinski A,
947 Stamatakis A, Song W, Su X, Szucsich NU, Tan M, Tan X, Tang M, Tang J,
948 Timelthaler G, Tomizuka S, Trautwein M, Tong X, Uchifune T, Walzl MG,
949 Wiegmann BM, Wilbrandt J, Wipfler B, Wong TK, Wu Q, Wu G, Xie Y, Yang S,
950 Yang Q, Yeates DK, Yoshizawa K, Zhang Q, Zhang R, Zhang W, Zhang Y, Zhao
951 J, Zhou C, Zhou L, Ziesmann T, Zou S, Li Y, Xu X, Zhang Y, Yang H, Wang J,
952 Wang J, Kjer KM, Zhou X. 2014. Phylogenomics resolves the timing and pattern
953 of insect evolution. *Science* **346:** 763–767.

954 Miyawaki S, Kuroki S, Maeda R, Okashita N, Koopman P, Tachibana M. 2020. The
955 mouse *Sry* locus harbors a cryptic exon that is essential for male sex determination.
956 *Science* **370**, 121–124.

957 Miyazaki S, Fujiwara K, Kai K, Masuoka Y, Gotoh H, Niimi T, Hayashi Y,
958 Shigenobu S, Maekawa K. 2021. Evolutionary transition of *doublesex* regulation in
959 termites and cockroaches: from sex-specific splicing to male-specific transcription.
960 *bioRxiv*.

961 Morita S, Ando T, Maeno A, Mizutani T, Mase M, Shigenobu S, Niimi T. 2019.
962 Precise staging of beetle horn formation in *Trypoxylus dichotomus* reveals the
963 pleiotropic roles of *doublesex* depending on the spatiotemporal developmental
964 contexts. *PLOS Genetics* **15:** e1008063.

965 Myosho T, Takehana Y, Hamaguchi S, Sakaizumi M. 2015. Turnover of sex
966 chromosomes in celebensis group medaka fishes. *G3: Genes, Genomes, Genetics*
967 **5:** 2685–2691.
968 Myosho T, Otake H, Masuyama H, Matsuda M, Kuroki Y, Fujiyama A, Naruse K,
969 Hamaguchi S, Sakaizumi M. 2012. Tracing the emergence of a novel sex-
970 determining gene in medaka, *Oryzias luzonensis*. *Genetics* **191:** 163–170.
971 Nanda I, Kondo M, Hornung U, Asakawa S, Winkler C, Shimizu A, Shan Z, Haaf T,
972 Shimizu N, Shima A, Schmid M, Schartl M. 2002. A duplicated copy of DMRT1
973 in the sex-determining region of the Y chromosome of the medaka, *Oryzias latipes*.
974 *PNAS* **99:** 11778–11783.
975 Ohbayashi F, Suzuki MG, Mita K, Okano K, Shimada T. 2001. A homologue of the
976 *Drosophila doublesex* gene is transcribed into sex-specific mRNA isoforms in the
977 silkworm, *Bombyx mori*. *Comparative Biochemistry and Physiology - Part B:*
978 *Biochemistry & Molecular Biology* **128:** 145–158.
979 Ohde T, Yaginuma T, Niimi T. 2011. Nymphal RNAi analysis reveals novel function
980 of scalloped in antenna, cercus and caudal filament formation in the firebrat,
981 *Thermobia domestica*. *Journal of Insect Biotechnology and Sericology* **80:** 101–
982 108.
983 Panara V, Budd GE, Janssen R. 2019. Phylogenetic analysis and embryonic
984 expression of panarthropod Dmrt genes. *Frontiers in Zoology* **16:** 1–18.
985 Pertea M, Pertea GM, Antonescu CM, Chang TC, Mendell JT, Salzberg SL. 2015.
986 StringTie enables improved reconstruction of a transcriptome from RNA-seq reads.
987 *Nature Biotechnology* **33:** 290–295.
988 Pomerantz AF, Hoy MA, Kawahara AY. 2015. Molecular characterization and
989 evolutionary insights into potential sex-determination genes in the western orchard

990 predatory mite *Metaseiulus occidentalis* (Chelicerata: Arachnida: Acari:
991 Phytoseiidae). *Journal of Biomolecular Structure and Dynamics* **33:** 1239–1253.
992 Raymond CS, Murphy MW, O'Sullivan MG, Bardwell VJ, Zarkower D. 2000. *Dmrt1*,
993 a gene related to worm and fly sexual regulators, is required for mammalian testis
994 differentiation. *Genes & Development* **14:** 2587–2595.
995 Raymond CS, Shamu CE, Shen MM, Seifert KJ, Hirsch B, Hodgkin J, Zarkower D.
996 1998. Evidence for evolutionary conservation of sex-determining genes. *Nature*,
997 **391**, 691–695.
998 R Core Team. 2020. *R: A language and environment for statistical computing*. R
999 Foundation for Statistical Computing.
1000 Robinson MD, McCarthy DJ, Smyth GK. 2010. edgeR: a Bioconductor package for
1001 differential expression analysis of digital gene expression data. *Bioinformatics* **26**:
1002 139–140.
1003 Romero-Pozuelo J, Foronda D, Martín P, Hudry B, Merabet S, Graba Y, Sánchez-
1004 Herrero E. 2019. Cooperation of axial and sex specific information controls
1005 Drosophila female genitalia growth by regulating the Decapentaplegic pathway.
1006 *Developmental Biology* **454:** 145–155.
1007 Rousset A., Bitsch C. 1993. Comparison between endogenous and exogenous yolk
1008 proteins along an ovarian cycle in the firebat *Thermobia domestica* (Insecta,
1009 Thysanura). *Comparative Biochemistry and Physiology Part B: Biochemistry and*
1010 *Molecular Biology***104:** 33–44.
1011 Sato Y, Shinka T, Sakamoto K, Ewis AA, Nakahori Y. 2010. The male-determining
1012 gene *SRY* is a hybrid of *DGCR8* and *SOX3*, and is regulated by the transcription
1013 factor *CP2*. *Molecular and Cellular Biochemistry* **337:** 267–275.

1014 Sharma A, Heinze SD, Wu Y, Kohlbrenner T, Morilla I, Brunner C, Wimmer EA, van
1015 de Zande L, Robinson MD, Beukeboom LW, Bopp D. 2017. Male sex in
1016 houseflies is determined by *Mdmd*, a paralog of the generic splice factor gene
1017 *CWC22*. *Science* **356:** 642–645.
1018 Shukla JN, Palli SR. 2012. Doublesex target genes in the red flour beetle, *Tribolium*
1019 *castaneum*. *Scientific Reports* **2:** 948.
1020 Sinclair AH, Berta P, Palmer MS, Hawkins JR, Griffiths BL, Smith MJ, Foster JW,
1021 Frischauf AM, Lovell-Badge R, Goodfellow PN. 1990. A gene from the human
1022 sex-determining region encodes a protein with homology to a conserved DNA-
1023 binding motif. *Nature* **346:** 240–244.
1024 Smith CA, Roeszler KN, Ohnesorg T, Cummins DM, Farlie PG, Doran TJ, Sinclair
1025 AH. 2009. The avian Z-linked gene *DMRT1* is required for male sex determination
1026 in the chicken. *Nature* **461:** 267–271.
1027 Suzuki MG, Funaguma S, Kanda T, Tamura T, Shimada T. 2003. Analysis of the
1028 biological functions of a *doublesex* homologue in *Bombyx mori*. *Developmental*
1029 *Genes and Evolution* **213:** 345–354.
1030 Suzuki MG, Imanishi S, Dohmae N, Nishimura T, Shimada T, Matsumoto S. 2008.
1031 Establishment of a novel in vivo sex-specific splicing assay system to identify a
1032 trans-acting factor that negatively regulates splicing of *Bombyx mori dsx* female
1033 exons. *Molecular and Cellular Biology* **28:** 333–343.
1034 Takaku Y, Suzuki H, Ohta I, Ishii D, Muranaka Y, Shimomura M, Hariyama T. 2013.
1035 A thin polymer membrane, nano-suit, enhancing survival across the continuum
1036 between air and high vacuum. *PNAS* **110:**7631–7635.

1037 Takahashi M, Okude G, Futahashi R, Takahashi Y, Kawata M. 2021. The effect of
1038 the *doublesex* gene in body colour masculinization of the damselfly *Ischnura*
1039 *senegalensis*. *Biology Lettters* **17:** 20200761.
1040 Takahashi M, Takahashi Y, Kawata M. 2019. Candidate genes associated with color
1041 morphs of female-limited polymorphisms of the damselfly *Ischnura senegalensis*.
1042 *Heredity* **122:** 81–92.
1043 Takehana Y, Matsuda M, Myosho T, Suster ML, Kawakami K, Shin-I T, Kohara Y,
1044 Kuroki Y, Toyoda A, Fujiyama A, Hamaguchi S, Sakaizumi M, Naruse K. 2014.
1045 Co-option of *Sox3* as the male-determining factor on the Y chromosome in the fish
1046 *Oryzias dancena*. *Nature Communications* **5:** 4157.
1047 Thongsaiklaing T, Passara H, Nipitwathanaphon M, Ngernsiri L. 2018. Identification
1048 and characterization of *doublesex* from the pumpkin fruit fly, *Bactrocera tau*
1049 (Diptera: Tephritidae). *European Journal of Entomology* **115:** 602–613.
1050 True JR, Carroll SB. 2002. Gene co-option in physiological and morphological
1051 evolution. *Annual Review of Cell and Developmental Biology* **18:** 53–80.
1052 Untergasser A, Cutcutache I, Koressaar T, Ye J, Faircloth BC, Remm M, Rozen SG.
1053 2012. Primer3--new capabilities and interfaces. *Nucleic Acids Research* **40:** e115.
1054 Verhulst EC, van de Zande L. 2015. Double nexus—Doublesex is the connecting
1055 element in sex determination. *Briefings in Functional Genomics* **14:** 396–406.
1056 Verhulst EC, van de Zande L, Beukeboom LW. 2010. Insect sex determination: it all
1057 evolves around *transformer*. *Current Opinion in Genetics & Development* **20:**
1058 376–383.
1059 Wexler J, Delaney EK, Belles X, Schal C, Wada-Katsumata A, Amicucci MJ, Kopp
1060 A. 2019. Hemimetabolous insects elucidate the origin of sexual development via
1061 alternative splicing. *eLife* **8:** e47490.

1062 Wexler JR, Plachetzki DC, Kopp A. 2014. Pan-metazoan phylogeny of the DMRT
1063 gene family: a framework for functional studies. *Developmental Genes and*
1064 *Evolution* **224:** 175−181.

1065 Wilkins AS. 1995. Moving up the hierarchy: a hypothesis on the evolution of a
1066 genetic sex determination pathway. *Bioessays* **17:** 71–77.

1067 Xu J, Chen S, Zeng B, James AA, Tan A, Huang Y. 2017. *Bombyx mori P-element*
1068 *Somatic Inhibitor* (*BmPSI*) is a key auxiliary factor for silkworm male sex
1069 determination. *PLoS Genet*ics **13:** e1006576.

1070 Xu J, Yu Y, Chen K, Huang Y. 2019. *Intersex* regulates female external genital and
1071 imaginal disc development in the silkworm. *Insect Biochemistry and Molecular*
1072 *Biology* **108:** 1–8.

1073 Xu J, Zhan S, Chen S, Zeng B, Li Z, James AA, Tan A, Huang Y. Sexually dimorphic
1074 traits in the silkworm, *Bombyx mori*, are regulated by *doublesex*. 2017. *Insect*
1075 *Biochemistry and Molecular Biology* **80:** 42–51.

1076 Yang Y, Zhang W, Bayrer JR, Weiss MA. 2008. Doublesex and the regulation of
1077 sexual dimorphism in *Drosophila melanogaster*: structure, function, and
1078 mutagenesis of a female-specific domain. *Journal of Biological Chemistry* **283:**
1079 7280–7292.

1080 Yoshimoto S, Okada E, Umemoto H, Tamura K, Uno Y, Nishida-Umehara C,
1081 Matsuda Y, Takamatsu N, Shiba T, Ito M. 2008. A W-linked DM-domain gene,
1082 *DM-W*, participates in primary ovary development in *Xenopus laevis*. *PNAS* **105:**
1083 2469–2474.

1084 Zhang HH, Xie YC, Li HJ, Zhuo JC, Zhang CX. 2021. Pleiotropic roles of the
1085 orthologue of the *Drosophila melanogaster Intersex* gene in the brown
1086 planthopper. *Genes* **12:** 379.
1087 Zhuo JC, Hu QL, Zhang HH, Zhang MQ, Jo SB, Zhang CX. 2018. Identification and
1088 functional analysis of the doublesex gene in the sexual development of a
1089 hemimetabolous insect, the brown planthopper. *Insect Biochemistry and Molecular*
1090 *Biology* **102:** 31–42.

1091

1092 # Video

1093 **Video 1. Time-lapse imaging of molting of *Thermobia domestica*.**

1094

Tables

Table 1. Taxa and proteins used for molecular phylogenetic analysis of DMRT family.

OTU name	gene	accession number	species	Order	Class/Subphylum	genome region	genome resource
Aasp_Dsx-like	*dsx-like*	GAZQ02010078.1	*Aretaon asperrimus*	Phasmatodea	Ectognatha/Hexapoda		
Afra_Dsx3	*dsx3*	AWC26109.1	*Artemia franciscana*	Anostraca	Brachiopoda/Crustacea		
Afra_Dsx4	*dsx4*	AWC26111.1	*Artemia franciscana*	Anostraca	Brachiopoda/Crustacea		
Annu_Dmrt99B	*dmrt99B*	GATX01081132.1	*Annulipalpia* sp.	Trichoptera	Ectognatha/Hexapoda		
Annu_Dsx	*dsx*	GATX01084595.1	*Annulipalpia* sp.	Trichoptera	Ectognatha/Hexapoda		
Aros_Dsx	*dsx*	XP_012262263.1	*Athalia rosae*	Hymenoptera	Ectognatha/Hexapoda		
Baet_Dsx-like	*dsx-like*	GATU02014641.1	*Baetis* sp.	Ephemeroptera	Ectognatha/Hexapoda		
Bdor_Dsx	*dsx*	AAB99948.1	*Bactrocera dorsalis*	Diptera	Ectognatha/Hexapoda		
Bger_Dsx	*dsx*	PSN43312.1	*Blattella germanica*	Dictyoptera	Ectognatha/Hexapoda		
Bhye_Dsx	*dsx*	GAYK02032082.1	*Boreus hyemalis*	Mecoptera	Ectognatha/Hexapoda		
Bmor_Dmrt11E	*dmrt11E*	XP_004930266.1	*Bombyx mori*	Lepidoptera	Ectognatha/Hexapoda		
Bmor_Dmrt93B	*dmrt93B*	XP_004932028.3	*Bombyx mori*	Lepidoptera	Ectognatha/Hexapoda		
Bmor_Dmrt99B	*dmrt99B*	XP_004924389.2	*Bombyx mori*	Lepidoptera	Ectognatha/Hexapoda		
Bmor_Dsx	*dsx*	XP_012544211.1	*Bombyx mori*	Lepidoptera	Ectognatha/Hexapoda		
Bmut_Dmrt1	*dmrt1*	ELR53308.1	*Bos mutus*	Cetartiodactyla	Mammalia/Vertebrata		
Btau_Dmrt2	*dmrt2*	XP_005210039.1	*Bos taurus*	Cetartiodactyla	Mammalia/Vertebrata		
Btry_Dsx	*dsx*	AAV85890.1	*Bactrocera tryoni*	Diptera	Ectognatha/Hexapoda		
Caqu_Dsx	*dsx*	CAQU003748-RA	*Catajapyx aquilonaris*	Diplura	Entognatha/Hexapoda		
Ccap_Dsx	*dsx*	XP_012158607.1	*Ceratitis capitata*	Diptera	Entognatha/Hexapoda		
Ccor_Dsx	*dsx*	GATG02018436.1	*Corydalus cornutus*	Megaloptera	Ectognatha/Hexapoda		
Ceut_Dmrt11E	*dmrt11E*	GAUX02031275.1	*Ceuthophilus* sp.	Orthoptera	Ectognatha/Hexapoda		
Cfel_Dsx	*dsx*	GAYP02016500.1	*Ctenocephalides felis*	Siphonaptera	Ectognatha/Hexapoda		
Cgal_Dsx	*dsx*	GAWK02011923.1	*Ceratophyllus gallinae*	Siphonaptera	Ectognatha/Hexapoda		
Choo_Dmrt11E	*dmrt11E*	NQII01002646.1	*Clitarchus hookeri*	Phasmatodea	Ectognatha/Hexapoda		
Choo_Dsx-like	*dsx-like*	NQII01000109.1	*Clitarchus hookeri*	Phasmatodea	Ectognatha/Hexapoda		
Dcar_Dsx1	*dsx1*	AIL86779.1	*Daphnia carina*	Diplostraca	Brachiopoda/Crustacea		
Dcar_Dsx2	*dsx2*	AIL86780.1	*Daphnia carina*	Diplostraca	Brachiopoda/Crustacea		
Dgal_Dsx1	*dsx1*	BAM33609.1	*Daphnia galeata*	Diplostraca	Brachiopoda/Crustacea		
Dgal_Dsx2	*dsx2*	BAM33610.1	*Daphnia galeata*	Diplostraca	Brachiopoda/Crustacea		
Dmag_Dmrt11E	*dmrt11e*	BAG12871.1	*Daphnia magna*	Diplostraca	Brachiopoda/Crustacea		

Dmag_Dmrt93B	*dmrt93b*	BAG12872.1	*Daphnia magna*	Diplostraca	Brachiopoda/Crustacea		
Dmag_Dmrt99B	*dmrt99b*	BAG12873.1	*Daphnia magna*	Diplostraca	Brachiopoda/Crustacea		
Dmag_Dsx1	*dsx1*	BAJ78307.1	*Daphnia magna*	Diplostraca	Brachiopoda/Crustacea		
Dmag_Dsx2	*dsx2*	BAJ78309.1	*Daphnia magna*	Diplostraca	Brachiopoda/Crustacea		
Dmel_Dmrt11E	*dmrt11e*	NP_511146.2	*Drosophila melanogaster*	Diptera	Ectognatha/Hexapoda		
Dmel_Dmrt93B	*dmrt93b*	NP_524428.1	*Drosophila melanogaster*	Diptera	Ectognatha/Hexapoda		
Dmel_Dmrt99B	*dmrt99b*	NP_524549.1	*Drosophila melanogaster*	Diptera	Ectognatha/Hexapoda		
Dmel_Dsx	*dsx*	NP_731197.1	*Drosophila melanogaster*	Diptera	Ectognatha/Hexapoda		
Dpul_Dsx1	*dsx1*	AGJ52190.1	*Daphnia pulex*	Diplostraca	Brachiopoda/Crustacea		
Dpul_Dsx2	*dsx2*	BAM33608.1	*Daphnia pulex*	Diplostraca	Brachiopoda/Crustacea		
Drer_Dmrt1	*dmrt1*	AAQ04555.1	*Danio rerio*	Cyprinifo rmes	Actinopterygii/Vertebrata		
Drer_Dmrt2	*dmrt2*	NP_571027.1	*Danio rerio*	Cyprinifo rmes	Actinopterygii/Vertebrata		
Edan_dmrt11E	*dmrt11E*	EDAN008414-RA	*Ephemera danica*	Ephemeroptera	Ectognatha/Hexapoda		
Edan_dmrt93B	*dmrt93B*	EDAN004527-RA	*Ephemera danica*	Ephemeroptera	Ectognatha/Hexapoda		
Edan_dmrt99B	*dmrt99B*	EDAN010669-RA	*Ephemera danica*	Ephemeroptera	Ectognatha/Hexapoda		
Edan_Dsx-like	*dsx-like*		*Ephemera danica*	Ephemeroptera	Ectognatha/Hexapoda	ephdan_Scaffold23	i5k
Eins_Dsx-like	*dsx-like*	GCCL01024227.1	*Ecdyonurus insignis*	Ephemeroptera	Ectognatha/Hexapoda		
Enos_Dsx	*dsx*	GAXW02019001.1	*Euroleon nostras*	Neuroptera	Ectognatha/Hexapoda		
Epen_Dsx	*dsx*	GAWT02033840.1	*Empusa pennata*	Mantodea	Ectognatha/Hexapoda		
Esup_Dsx	*dsx*	GAVW02000373.1	*Epiophlebia superstes*	Odonata	Ectognatha/Hexapoda		
Eury_Dmrt11E	*dmrt11E*	GAZG02011227.1	*Eurylophella* sp.	Ephemeroptera	Ectognatha/Hexapoda		
Eury_Dsx-like	*dsx-like*	GAZG02000044.1	*Eurylophella* sp.	Ephemeroptera	Ectognatha/Hexapoda		
Focc_Dsx	*dsx*	FOCC007514-RA	*Frankliniella occidentalis*	Thysanoptera	Ectognatha/Hexapoda		
Gcor_Dsx	*dsx*	BAW32683.1	*Gnatocerus cornutus*	Coleoptera	Ectognatha/Hexapoda		
Harm_Dsx	*dsx*	XP_021192052.1	*Helicoverpa armigera*	Lepidoptera	Ectognatha/Hexapoda		
Hdeu_Dsx	*dsx*	maker-scaffold37size976698-augustus-gene-4.5-mRNA-1	*Holacanthella duospinosa*	Collembola	Entognatha/Hexapoda		i5k
Hydr_Dsx	*dsx*	GAVM02014074.1	*Hydroptila* sp.	Trichoptera	Ectognatha/Hexapoda		
Ibic_Dsx-like	*dsx-like*	GAXA02007870.1	*Isonychia bicolor*	Ephemeroptera	Ectognatha/Hexapoda		
Icra_Dsx	*dsx*	GAZH02011000.1	*Inocellia crassicornis*	Raphidioptera	Ectognatha/Hexapoda		
Lcup_Dmrt11E	*dmrt11E*	XP_023291847.1	*Lucilia cuprina*	Diptera	Ectognatha/Hexapoda		i5k
Lcup_Dmrt93B	*dmrt93B*	XP_023302612.1	*Lucilia cuprina*	Diptera	Ectognatha/Hexapoda		
Lcup_Dmrt99B	*dmrt99B*	XP_023308885.1	*Lucilia cuprina*	Diptera	Ectognatha/Hexapoda		
Lcup_Dsx	*dsx*	ADG37648.1	*Lucilia cuprina*	Diptera	Ectognatha/Hexapoda		
Lful_Dsx	*dsx*	LFUL018497-RA	*Ladona fulva*	Odonata	Ectognatha/Hexapoda		

Lmig_Dsx	*dsx*		*Locusta migratoria*	Orthoptera	Ectognatha/Hexapoda	scaffold3427	NCBI
Mdom_Dmrt11E	*dmrt11E*	XP_019890834.1	*Musca domestica*	Diptera	Ectognatha/Hexapoda		
Mdom_Dmrt99B	*dmrt99B*	XP_005186857.1	*Musca domestica*	Diptera	Ectognatha/Hexapoda		
Mdom_Dsx	*dsx*	AAR23813.1	*Musca domestica*	Diptera	Ectognatha/Hexapoda		
Mext_Dmrt99B	*dmrt99B*	Medex_00095964-RA	*Medauroidea extradentata*	Phasmatodea	Ectognatha/Hexapoda		
Mext_Dsx	*dsx*		*Medauroidea extradentata*	Phasmatodea	Ectognatha/Hexapoda	PNEQ01023967.1 [32614-32324]	i5k
Mext_Dsx-like	*dsx-like*	Medex_00099178-RA	*Medauroidea extradentata*	Phasmatodea	Ectognatha/Hexapoda	PNEQ01097711.1 [2988-3275]	i5k
Mfas_Dsx	*dsx*	GCNI01018035.1	*Meroplius fasciculatus*	Diptera	Ectognatha/Hexapoda		
Mmac_Dsx	*dsx*	BAM33613.1	*Moina macropaeneus*	Diplostraca	Brachiopoda/Crustacea		
Mmus_Dmrt1	*dmrt1*	AAO41736.1	*Mus musculus*	Rodentia	Mammalia/Vertebrata		
Mrel_Dsx	*dsx*	GASW02021994.1	*Mantis religiosa*	Mantodea	Ectognatha/Hexapoda		
Mviol_Dsx	*dsx*	GATA02010186.1	*Meloe violaceus*	Coleoptera	Ectognatha/Hexapoda		
Ofur_Dsx	*dsx*	AHF81635.1	*Ostrinia furnacalis*	Lepidoptera	Ectognatha/Hexapoda		i5k
Otau_Dsx	*dsx*	AEX92938.1	*Onthophagus taurus*	Coleoptera	Ectognatha/Hexapoda		
Ppra_Dsx	*dsx*	GAVV02027199.1	*Pseudomalla da prasinus*	Neuroptera	Ectognatha/Hexapoda		
Psch_Dsx-like	*dsx-like*	GAWJ02028457.1	*Peruphasma schultei*	Phasmatodea	Ectognatha/Hexapoda		i5k
Smag_Dmrt99B	*dmrt99b*	GEYQ01032489.1	*Steganacarus magnus*	Oribatida	Arachnida/Chelicerata		
Tcas_Dmrt93B	*dmrt93B*	XP_008199135.1	*Tribolium castaneum*	Coleoptera	Ectognatha/Hexapoda		
Tcas_Dmrt99B	*dmrt99B*	XP_975675.1	*Tribolium castaneum*	Coleoptera	Ectognatha/Hexapoda		
Tcas_Dsx	*dsx*	NP_001345539.1	*Tribolium castaneum*	Coleoptera	Ectognatha/Hexapoda		
Tcri_Dsx-like	*dsx-like*	GAVX02010884.1	*Timema cristinae*	Phasmatodea	Ectognatha/Hexapoda		
Tdic_Dsx	*dsx*	BAM93340.1	*Trypoxylus dichotomus*	Coleoptera	Ectognatha/Hexapoda		
Tdom_Dmrt11E	*dmrt11E*	this study	*Thermobia domestica*	Zygentoma	Ectognatha/Hexapoda	scaffold42162_cov39 [159031-158906]	
Tdom_Dmrt93B	*dmrt93B*	this study	*Thermobia domestica*	Zygentoma	Ectognatha/Hexapoda	scaffold1624327_cov47 [121390-121265]	
Tdom_Dmrt99B	*dmrt99B*	this study	*Thermobia domestica*	Zygentoma	Ectognatha/Hexapoda	scaffold21840_cov24 [214972-214787]	
Tdom_Dsx	*dsx*	this study	*Thermobia domestica*	Zygentoma	Ectognatha/Hexapoda		
Tdom_Dsx-like	*dsx-like*	this study	*Thermobia domestica*	Zygentoma	Ectognatha/Hexapoda	scaffold27567_cov49 [365805-281362]	
Tger_Dsx-like	*dsx-like*	GASO02037568.1	*Tricholepidion gertschi*	Zygentoma	Ectognatha/Hexapoda		
Tsub_Dsx	*dsx*	GASQ02027559.1	*Tetrix subulata*	Orthoptera	Ectognatha/Hexapoda		
Xant_Dsx	*dsx*	GAUI02048130.1	*Xanthostigma* sp.	Raphidioptera	Ectognatha/Hexapoda		
Xlae_Dmrt1	*dmrt1*	NP_001089969.1	*Xenopus laevis*	Anura	Amphibia/Vertebrata		
Xlae_Dmrt4	*dmrt4*	AAH70678.2	*Xenopus laevis*	Anura	Amphibia/Vertebrata		
Xlae_Dmrt5	*dmrt5*	AAI70166.1	*Xenopus laevis*	Anura	Amphibia/Vertebrata		

1098

Table 2. Results of RT-qPCR assay and Brunner–Munzel test. Significant levels are indicated by asterisks in significance column: *$P < 0.05$, **$P < 0.01$, ***$P < 0.001$. n.s. means non-significance.

experiment	treatment	sample size (*N*)	median		proportion of $2^{-\Delta Ct}$	95% confidence interval		Brunner-Munzel test			*P*-value adjusted by Holm's method	significance	graph #
			ΔCt	$2^{-\Delta Ct}$				statistics	df	*P*-value			
dsx male-type expression level	male	12	8.59	2.66.E-03	1.00	0.83	1.07	8.25	12.82	1.75.E-06	-	***	Figure 1D
	female	8	13.89	6.64.E-05	0.02								
dsx female-type expression level	male	11	9.98	9.90.E-04	1.00	-0.01	0.01	-92.63	20.95	2.20.E-16	-	***	Figure 1D
	female	12	5.77	1.83.E-02	18.47								
dsx-like expression level	male	12	3.62	8.13.E-02	1.00	0.58	1.02	2.86	21.84	9.24.E-03	-	**	Figure 1E
	female	12	4.71	3.83.E-02	0.47								
dsx expression level in males	*egfp*	12	7.50	5.52.E-03	1.00								
	dsx all	8	9.24	1.66.E-03	0.30	0.45	1.03	1.78	13.61	9.68.E-02	1.94.E-01	n.s.	Figure 1–figure supplement 3B
	dsx-like	10	7.14	7.10.E-03	1.29	0.07	0.57	-1.54	17.40	1.43.E-01	1.43.E-01	n.s.	
dsx expression level in males excluding outliers	*egfp*	12	7.50	5.52.E-03	1.00								
	dsx all	7	9.32	1.57.E-03	0.28	0.64	1.05	3.64	13.87	2.73.E-03	5.45.E-03	**	Figure 1–figure supplement 3A
	dsx-like	10	7.14	7.10.E-03	1.29	0.07	0.57	-1.54	17.40	1.43.E-01	1.43.E-01	n.s.	
dsx expression level in females	*egfp*	10	5.18	2.76.E-02	1.00								
	dsx all	17	6.23	1.33.E-02	0.48	0.57	0.99	2.78	16.21	1.33.E-02	2.65.E-02	*	Figure 1–figure supplement 3A
	dsx-like	9	5.17	2.78.E-02	1.01	0.20	0.82	0.08	15.38	9.40.E-01	9.40.E-01	n.s.	
dsx-like expression level in males	*egfp*	12	5.72	1.95.E-02	1.00								
	dsx all	8	6.17	1.39.E-02	0.72	0.50	0.98	2.08	17.99	5.19.E-02	5.19.E-02	n.s.	Figure 1–figure supplement 3A
	dsx-like	10	10.17	8.68.E-04	0.04	1.00	1.00	Inf	NaN	2.20.E-16	4.40.E-16	***	
dsx-like expression level in females	*egfp*	10	6.08	1.49.E-02	1.00								
	dsx all	17	6.31	1.26.E-02	0.85	0.47	0.93	1.82	16.18	8.76.E-02	8.76.E-02	n.s.	Figure 1–figure supplement 3A
	dsx-like	9	11.58	3.27.E-04	0.02	1.00	1.00	Inf	NaN	2.20.E-16	4.40.E-16	***	

vitellogenin-1 expression level in males	*egfp*	5	15.00	3.06.E-05	1.00								Figure 4D
	dsx all	9	4.42	4.68.E-02	1530.72	-0.05	0.09	-15.20	10.67	1.44.E-08	2.87.E-08	***	
	dsx-like	7	10.18	8.62.E-04	28.18	-0.12	0.41	-3.09	8.42	1.39.E-02	1.39.E-02	*	
	dsx+dsx-like	9	4.28	5.14.E-02	1678.94	0.00	0.00	-Inf	NaN	2.20.E-16	6.60.E-16	***	
vitellogenin-2 expression level in males	*egfp*	3	16.76	9.01.E-06	1.00								Figure 4D
	dsx all	8	11.24	4.13.E-04	45.89	0.00	0.00	-Inf	NaN	2.20.E-16	6.60.E-16	***	
	dsx-like	5	15.48	2.19.E-05	2.43	-0.24	0.51	-2.46	5.56	5.24.E-02	6.19.E-01	n.s.	
	dsx+dsx-like	8	10.64	6.27.E-04	28.64	0.00	0.00	-Inf	NaN	2.20.E-16	6.60.E-16	***	
vitellogenin-3 expression level in males	*egfp*	10	11.28	4.21.E-04	1.00								Figure 4D
	dsx all	10	3.25	1.07.E-01	254.99	-0.09	0.23	-6.00	9.86	1.40.E-04	2.80.E-04	***	
	dsx-like	10	8.73	2.37.E-03	5.64	-0.03	0.39	-3.29	15.01	4.97.E-03	4.97.E-03	**	
	dsx+dsx-like	9	2.82	1.42.E-01	336.55	0.00	0.00	-Inf	NaN	2.20.E-16	6.60.E-16	***	
vitellogenin-1 expression level in females	*egfp*	8	-2.67	6.34.E+00	1.00								Figure 4E
	dsx all	10	-0.44	1.41.E+00	0.22	0.51	1.02	2.20	15.51	4.33.E-02	4.33.E-02	*	
	dsx-like	7	-0.29	1.22.E-00	0.19	0.70	1.08	4.55	10.89	8.51.E-04	2.56.E-03	**	
	dsx+dsx-like	8	0.90	5.40.E-01	0.09	0.58	1.10	3.00	8.82	1.52.E-02	3.05.E-02	*	
vitellogenin-2 expression level in females	*egfp*	8	1.84	2.80.E-01	1.00								Figure 4E
	dsx all	10	4.34	4.96.E-02	0.18	0.65	1.05	3.68	15.57	2.11.E-03	4.22.E-03	**	
	dsx-like	7	5.24	2.65.E-02	0.09	0.83	1.06	8.45	12.94	1.27.E-06	3.80.E-06	***	
	dsx+dsx-like	8	6.10	1.48.E-02	0.05	0.63	1.15	3.54	7.29	8.92.E-03	8.92.E-03	**	
vitellogenin-3 expression level in females	*egfp*	8	-3.37	1.03.E+01	1.00								Figure 4E
	dsx all	10	-1.98	3.95.E+00	0.38	0.65	1.07	3.75	11.23	3.12.E-03	6.23.E-03	**	
	dsx-like	8	0.84	7.82.E-01	0.08	0.81	1.06	7.56	12.60	4.98.E-06	1.49.E-05	***	
	dsx+dsx-like	8	0.05	1.09.E+00	0.11	0.57	1.13	2.95	7.56	1.97.E-02	1.97.E-02	*	

The source data of this table can be obtained in the Table2–source data 1 file.

Table 3. Results of Smirnov–Grubbs' test for expression level of *dsx* mRNA in nymphal RNAi males. The determination of whether a value is an outlier or not is based on the *P*-value and is shown in the "outlier?" column.

data	max/min	value	*G*	*U*	*P*-value	outlier?
egfp	max	10.45	1.8587	0.65738	2.73.E-01	no
	min	5.31	1.59672	0.74715	5.74.E-01	no
dsx	max	10.47	0.97	0.85	1.00.E+00	no
	min	5.23	2.27	0.15688	5.14.E-03	yes
dsx-like	max	7.70	1.01	0.88	1.00.E+00	no
	min	5.12	2.08	0.47	8.35.E-02	no
reanalysis of *dsx*	max	10.47	1.52	0.55	3.52.E-01	no
	min	8.44	1.42	0.61	4.70.E-01	no

Table 4. Results of generalized linear model of female traits. Significant levels are indicated by asterisks in significance column: *P<0.05, **P < 0.01, ***P < 0.001. n.s. means non-significance.

objective variable	sample size (N)	explanatory variables	LR Chisq	Df	*P*-value	significance	Fig #
ovipositor length	*egfp*: 10, *dsx* all: 17, *dsx-like*: 9, *dsx+dsx-like*: 12, total: 48	*dsx* RNAi	0.26	1	6.08.E-01	n.s.	Figure 2H
		dsx-like RNAi	0.58	1	4.47.E-01	n.s.	
		prothoracic width	297.00	1	2.00.E-16	***	
		dsx RNAi:*dsx-like* RNAi	2.67	1	1.02.E-01	n.s.	
ovipositor length	*egfp*: 8, *dsx all*: 8, *dsx male-type*: 7, *dsx female-type*: 13, total: 36	*dsx* all RNAi	1.29	1	2.56.E-01	n.s.	Figure 2–figure supplement 3
		dsx male-type RNAi	1.29	1	2.56.E-01	n.s.	
		dsx female-type RNAi	0.42	1	5.18.E-01	n.s.	
		prothoracic width	146.52	1	2.00.E-16	***	
prothoracic width	*egfp*: 10, *dsx* all: 17, *dsx-like*: 9, *dsx+dsx-like*: 13, total: 49	*dsx* RNAi	2.17	1	1.41.E-01	n.s.	Figure 2–figure supplement 4
		dsx-like RNAi	1.96	1	1.61.E-01	n.s.	
		dsx RNAi:*dsx-like* RNAi	2.16	1	1.41.E-01	n.s.	
previtellogenic oocyte number	*egfp*: 7, *dsx* all: 16, *dsx-like*: 10, *dsx+dsx-like*: 9, total: 42	*dsx* RNAi	0.08	1	7.83.E-01	n.s.	Figure 3D
		dsx-like RNAi	0.23	1	6.31.E-01	n.s.	
		prothoracic width	0.97	1	3.25.E-01	n.s.	

		dsx RNAi:*dsx-like* RNAi	0.06	1	8.10.E-01	n.s.	
early vitellogenic oocyte number	*egfp*: 7, *dsx* all: 16, *dsx-like*: 10, *dsx+dsx-like*: 9, total: 42	*dsx* RNAi	0.11	1	7.45.E-01	n.s.	Figure 3D
		dsx-like RNAi	0.08	1	7.77.E-01	n.s.	
		prothoracic width	3.50	1	6.14.E-02	n.s.	
		dsx RNAi:*dsx-like* RNAi	0.62	1	4.30.E-01	n.s.	
late vitellogenic oocyte number	*egfp*: 7, *dsx* all: 16, *dsx-like*: 10, *dsx+dsx-like*: 9, total: 42	*dsx* RNAi	0.46	1	5.00.E-01	n.s.	Figure 3D
		dsx-like RNAi	1.12	1	2.90.E-01	n.s.	
		prothoracic width	9.84	1	1.71.E-03	**	
		dsx RNAi:*dsx-like* RNAi	2.16	1	1.42.E-01	n.s.	
oocyte size	*egfp*: 5, *dsx* all: 9, *dsx-like*: 7, *dsx+dsx-like*: 2, total: 23	*dsx* RNAi	0.1689	1	6.81.E-01	n.s.	Figure3–figure supplement 3
		dsx-like RNAi	3.4291	1	6.41.E-02	n.s.	
		prothoracic width	4.273	1	3.87.E-02	*	
		dsx RNAi:*dsx-like* RNAi	1.4509	1	2.23.E-01	n.s.	

The source data of this table can be obtained in the Table4–source data 1 file.

Table 5. Results of generalized linear model of male traits. *P*-values are indicated by asterisks in significance column: ***P* < 0.01. n.s. means non-significance.

objective variable	sample size (*N*)	explanatory variables	LR Chisq	Df	*P*-value	significance	Fig #
sperm number	*egfp*: 9 *dsx* all: *6* *dsx-like*: 10 *dsx*+*dsx-like*: 4, total: 29	*dsx* RNAi	7.93	1	4.87.E-03	**	Figure 3C
		dsx-like RNAi	2.06	1	1.51.E-01	n.s.	
		prothoracic width	8.68	1	3.21.E-03	**	
		dsx RNAi:*dsx-like* RNAi	0.02	1	8.79.E-01	n.s.	
prothoracic width	*egfp*: 12, *dsx* all: *8, dsx-like*: 10, *dsx*+*dsx-like*: 6, total: 36	*dsx* RNAi	0.03	1	8.71.E-01	n.s.	Figure 2–figure supplement 4
		dsx-like RNAi	2.82	1	9.31.E-02	n.s.	
		dsx RNAi:*dsx-like* RNAi	1.09	1	2.96.E-01	n.s.	

The source data of this table can be obtained in the Table5–source data 1 file.

1115 **Table 6. Primers' list used in this study.**

No.	expeiment	target	primer name	primer sequence (5' to 3')	length	note
1	5' RACE	*doublesex* (*dsx*)	Tdom_*dsx*_RACE_01	TCGCGTGACAAGGAAGAAGGCCCCGG	26	gene specific primer
2	5' RACE	*dsx*	Tdom_*dsx*_RACE_02	AGGCCCCGGAATTGAAGAAGCACCT	25	nested gene specific primer
3	5' RACE	*doublesex-like* (*dsx-like*)	Tdom_*dsx-like*_RACE_01	CACTTTGAAAACGCAGGGCTGGATG	25	gene specific primer
4	5' RACE	*dsx-like*	Tdom_*dsx-like*_RACE_02	GGGCTGGATGTTCGCTGTAGTTGAA	25	nested gene specific primer
5	3' RACE	*dsx*	Tdom_*dsx*_RACE_03	GCTTCTTCAATTCCGGGGCCTTCTTCC	27	gene specific primer
6	3' RACE	*dsx*	Tdom_*dsx*_RACE_04	TCAATTCCGGGGCCTTCTTCCTTGTCA	27	nested gene specific primer
7	3' RACE	*dsx-like*	Tdom_*dsx-like*_RACE_03	AGACAGCAGCCAAATGACGTCAAGA	25	gene specific primer
8	3' RACE	*dsx-like*	Tdom_*dsx-like*_RACE_04	ACAGCAGCCAAATGACGTCAAGAGA	25	nested gene specific primer
9	RT-qPCR	*ribosomal protein 49* (*rp49*)	Tdom_*rp49*_RT-qPCR_F	ACCCACCATAGTCAAGAAGCGGA	23	reference gene
10	RT-qPCR	*ribosomal protein 49* (*rp49*)	Tdom_*rp49*_RT-qPCR_R	AACTGTCCCTTAAACCGCCTTCG	23	reference gene
11	RT-qPCR	*dsx* male-specific region	Tdom_*dsx*_male_RT-qPCR_F	GCTACCGCTTGAAACATTGCCTT	23	
12	RT-qPCR	*dsx* male-specific region	Tdom_*dsx*_male_RT-qPCR_R	AGTGCCATGGATCGTAATTCTGCT	24	
13	RT-qPCR	*dsx* female-specific region	Tdom_*dsx*_female_RT-qPCR_F	CTACCGCTTGAAACATTGCCTTT	23	
14	RT-qPCR	*dsx* female-specific region	Tdom_*dsx*_female_RT-qPCR_R	TGCCCTGATTCATGCATTGA	20	
15	RT-qPCR	*dsx* common region	Tdom_*dsx*_RT-qPCR_F	ACCCAGCCATGCCTCCTAATGTA	23	
16	RT-qPCR	*dsx* common region	Tdom_*dsx*_RT-qPCR_R	CTTCGAGCGTCCTTCAGAACGAC	23	
17	RT-qPCR	*dsx-like*	Tdom_*dsx-like*_RT-qPCR_F	ACGGGTTGTTGCTTTACATCTGT	23	
18	RT-qPCR	*dsx-like*	Tdom_*dsx-like*_RT-qPCR_R	TCTCTTGACGTCATTTGGCTGCT	23	
19	RT-qPCR	*vitellogenin-1*	Tdom_*vitellogenin-1*_RT-qPCR_F	TGCTCCATTCAACAACCAGC	20	

20	RT-qPCR	*vitellogenin-1*	Tdom_*vitellogenin-1*_RT-qPCR_R	AGCCCAGATGAACTTGACGA	20	
21	RT-qPCR	*vitellogenin-2*	Tdom_*vitellogenin-2*_RT-qPCR_F	CCAGTGATGGTGGCAATTCAGGA	23	
22	RT-qPCR	*vitellogenin-2*	Tdom_*vitellogenin-2*_RT-qPCR_R	TGTGGCTGTGACTGTCGTTTTGT	23	
23	RT-qPCR	*vitellogenin-3*	Tdom_*vitellogenin-3*_RT-qPCR_F	CACCAGCGATGTTGACGAGAAGA	23	
24	RT-qPCR	*vitellogenin-3*	Tdom_*vitellogenin-3*_RT-qPCR_R	GCTCAAACTCAGGCTCAAGTGGA	23	
25	dsRNA	*egfp*	*egfp*_dsRNA_F	ATCATGGCCGACAAGCAGAA	20	control of RNAi assay
26	dsRNA	*egfp*	*egfp*_dsRNA_R	AACTCCAGCAGGACCATGTG	20	control of RNAi assay
29	dsRNA	*dsx* common region	Tdom_*dsx*_dsRNA_F	CCAAGCCCAAGACGAAGC	18	
30	dsRNA	*dsx* common region	Tdom_*dsx*_dsRNA_R	CCGACTGTTACATTAGGAGGC	21	
31	dsRNA	*dsx* male-specific region	Tdom_*dsx*_male-type_dsRNA_F	GCAGAATTACGATCCATGGCAC	22	
32	dsRNA	*dsx* male-specific region	Tdom_*dsx*_male-type_dsRNA_R	CGTACTGGCCCTTTACATGGT	21	
33	dsRNA	*dsx* female-specific region	Tdom_*dsx*_female-type_dsRNA_F	TGCATGAATCAGGGCATTATTG	22	
34	dsRNA	*dsx* female-specific region	Tdom_*dsx*_female-type_dsRNA_R	TCAATTGATCTGACTTGTGCCT	22	
35	dsRNA	*dsx-like*	Tdom_*dsx-like*_dsRNA_F	CTCATGTGCAGTGATGTGGC	20	
36	dsRNA	*dsx-like*	Tdom_*dsx-like*_dsRNA_R	TGCGTCAATGAACAGCGAAA	20	
37	dsRNA	pCR4-TOPO vector	T7-pCR4-TOPO_F	taatacgactcactatagggAGACCACGTCCTGCAGGTTTAAACG	45	T7 flanked
38	dsRNA	pCR4-TOPO vector	T7-pCR4-TOPO_R	taatacgactcactatagggAGACCACCGAATTGAATTTAGCGGC	45	T7 flanked

1116

Figure Supplements

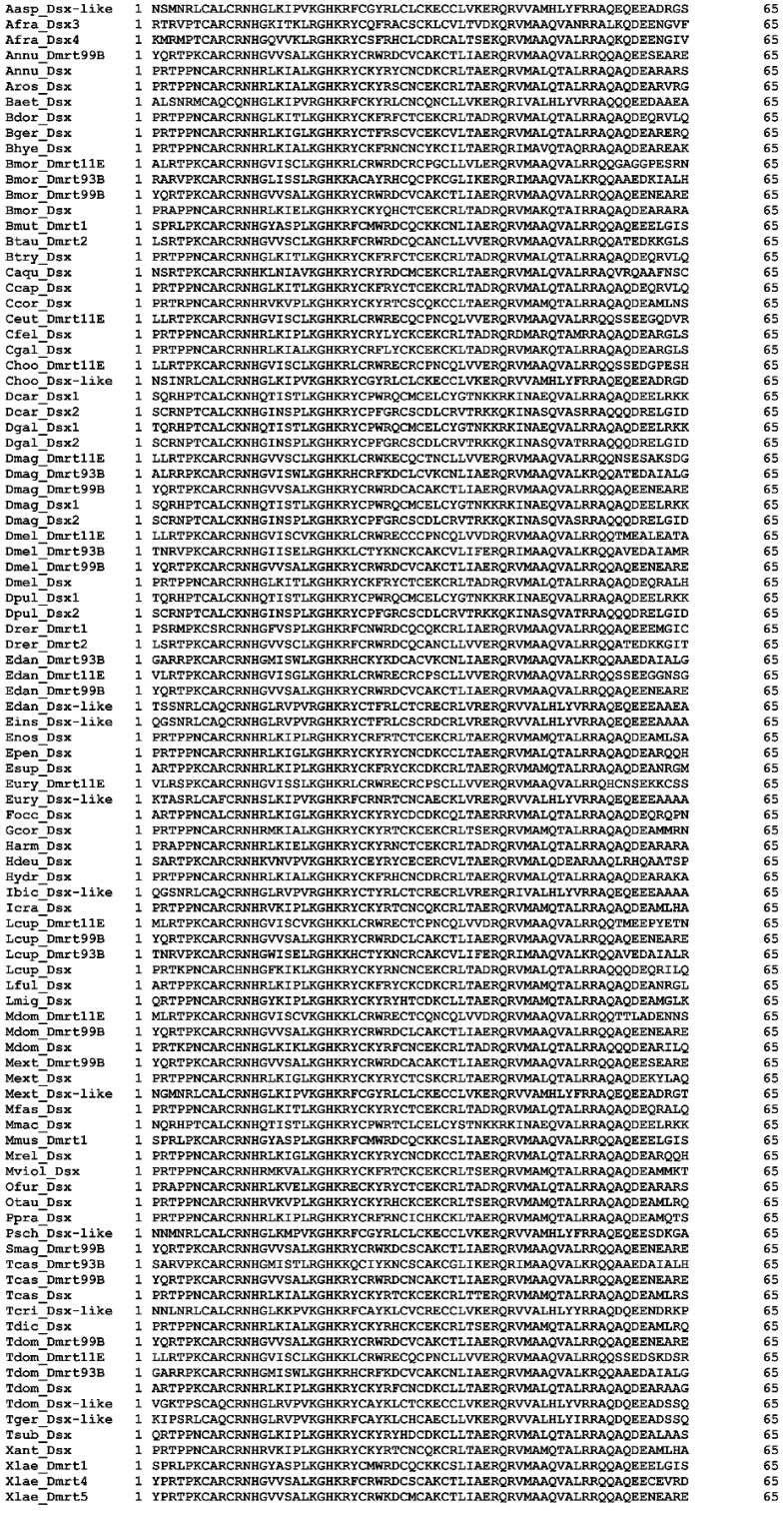

Figure 1–figure supplement 1. Multiple sequence alignment of DM domain of DMRT family proteins for molecular phylogenetic analysis. The 65 amino acids of 97 DMRT proteins were used for the molecular phylogenetic analysis.

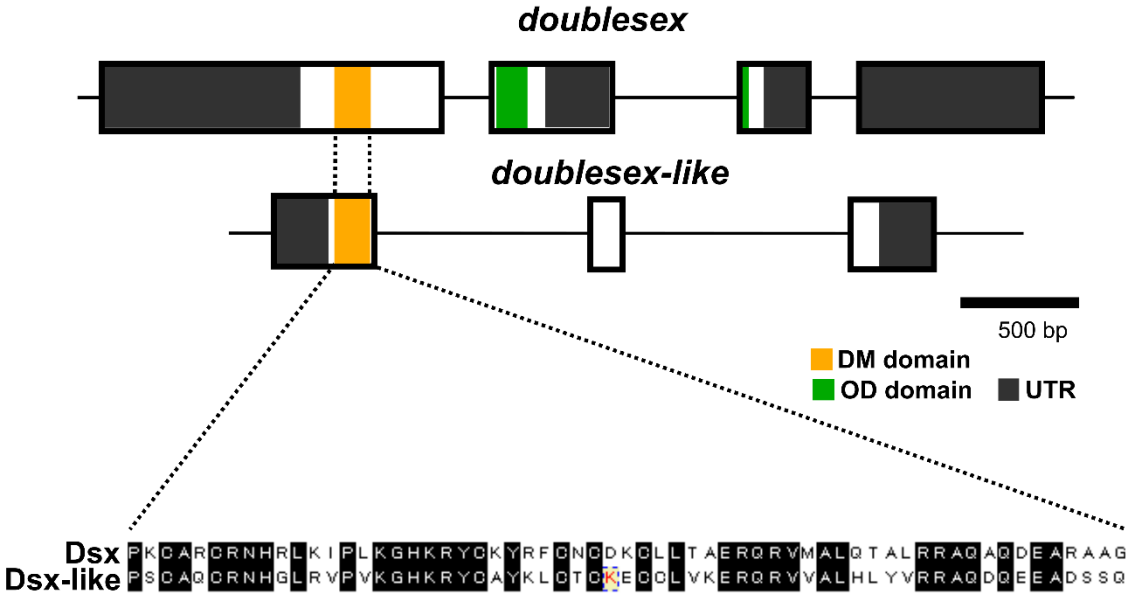

Figure 1–figure supplement 2. Comparison of DM domain sequences between Dsx and Dsx-like. The upper figures show the gene structures of *dsx* and *dsx-like*, and the lower one is the result of the multiple sequence alignment of the DM domain in Dsx and Dsx-like of *Thermobia domestica*. The black-highlighted sequences are shared in both proteins.

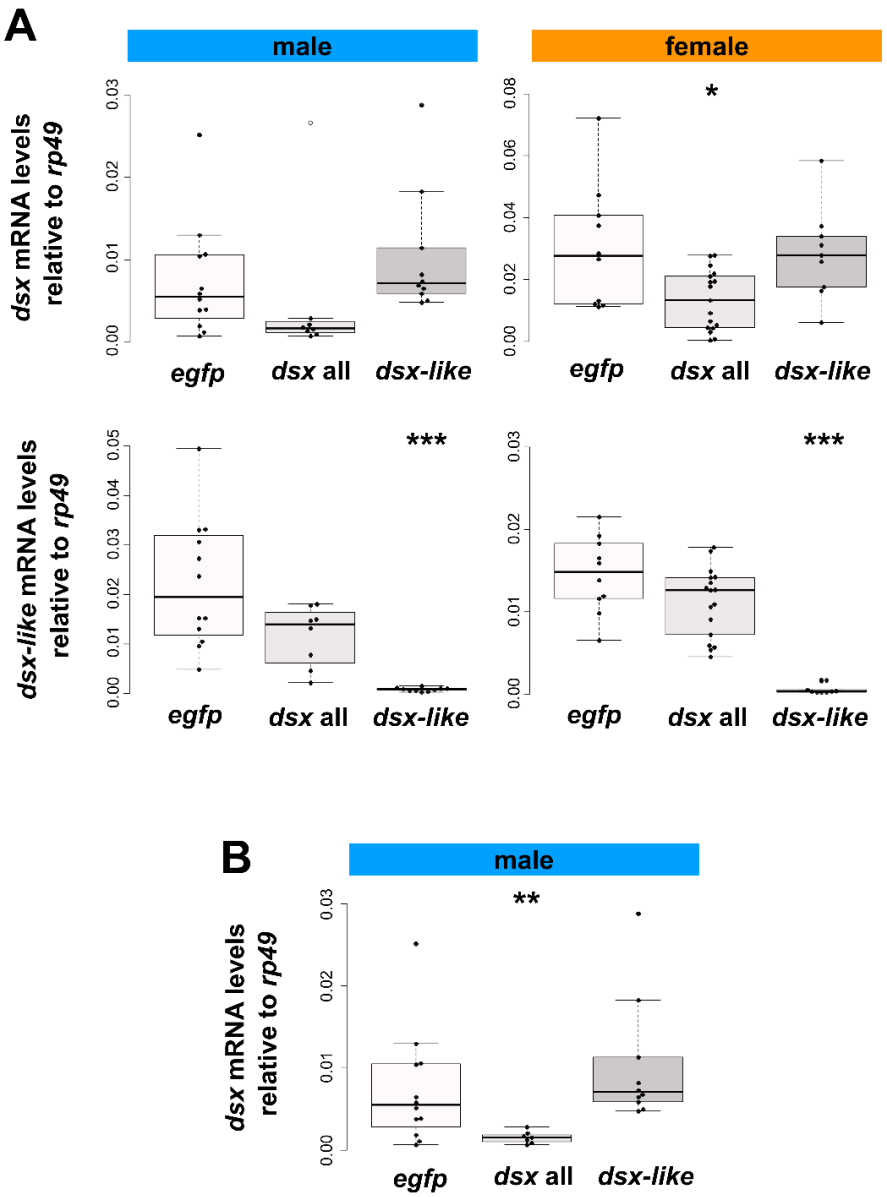

Figure 1–figure supplement 3. Expression of *dsx* and *dsx-like* mRNA in nymphal RNAi individuals. (A) results of RT-qPCR assay. The expression profiles of *dsx* and *dsx-like* mRNA were analyzed by RT-qPCR assay and are indicated by their expression level relative to the expression of a reference gene (*ribosomal protein 49*). The upper graphs are the expression of *dsx* mRNA and the lower ones are that of *dsx-like* mRNA. The left column is the result in males and the right one is that in females. (B**)** the expression level of *dsx* mRNA in the nymphal RNAi males after excluding an outlier. To test the outlier, the Smirnov–Grubbs' test was performed. Results of the Smirnov–Grubbs' test are shown in Table 3. Results of the Brunner–Munzel test are indicated by asterisks: **P* < 0.05; ***P* < 0.01; ****P* < 0.001 and is also described in Table 2. *P* > 0.05 is not shown. Each plot is an individual. White plot is the outlier. Sample size are listed in Table 2.

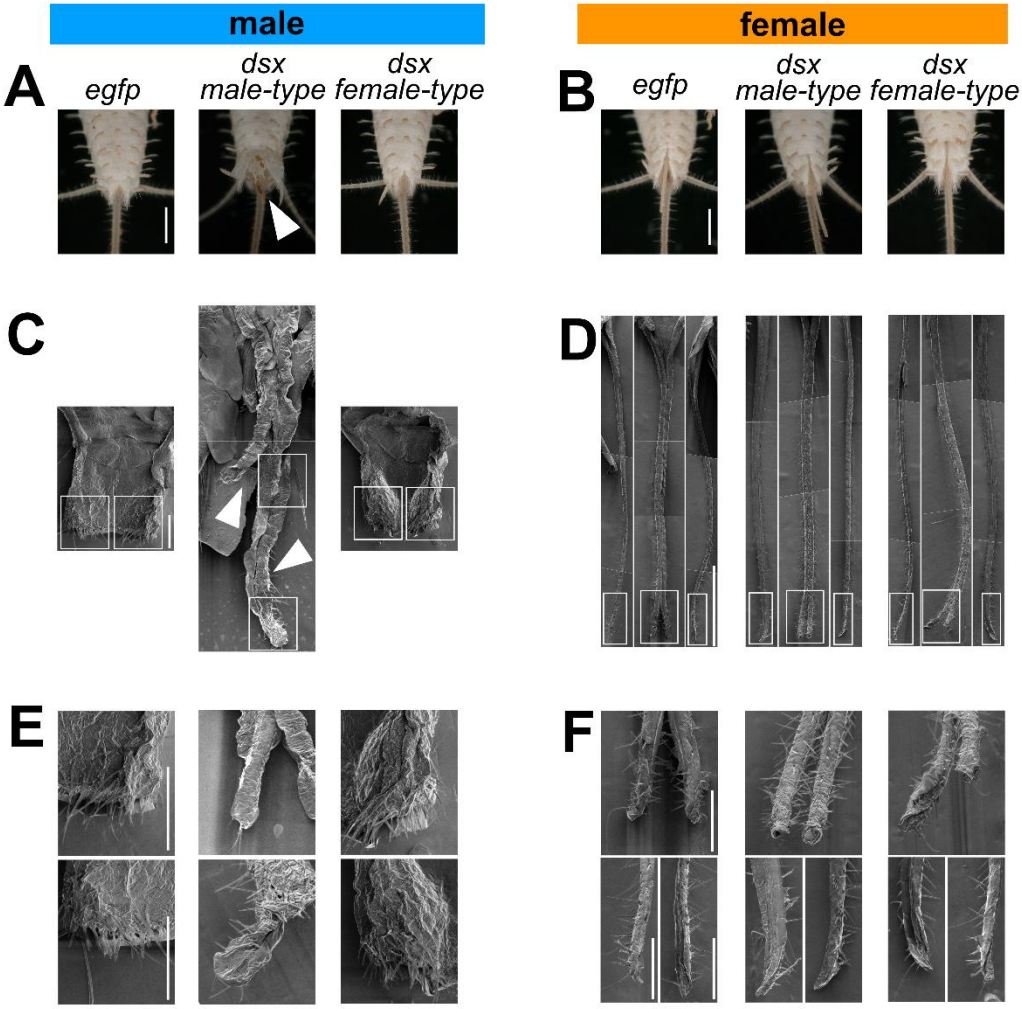

Figure 2–figure supplement 1. External genital organs of nymphal RNAi individuals. (A) The penis in ventral view of *dsx* male or female-type RNAi males. (B) The ovipositor in ventral view of *dsx* male or female-type RNAi females. (C) SEM images of the male penis or the ovipositor-like organ. White frames are the areas shown in (E). (D) SEM images of the female ovipositor. Each image is separated into three parts. The left and right image is each lobe of the valvula I. The middle image is the valvula II. White frames are the areas showed in (F). (E) Higher magnification SEM images of the male genital organ in (C). Each image shows the higher magnification view of the area enclosed by the white frame in (C). (F) Higher magnification SEM images of the ovipositor. Each image shows the higher magnification view of the area enclosed by the white frame in (*D*). The arrowheads show the ovipositor-like organ in the *dsx* male-type RNAi male. Scales: 1000 μm (A, B, and D), 100 μm (C, E, and F).

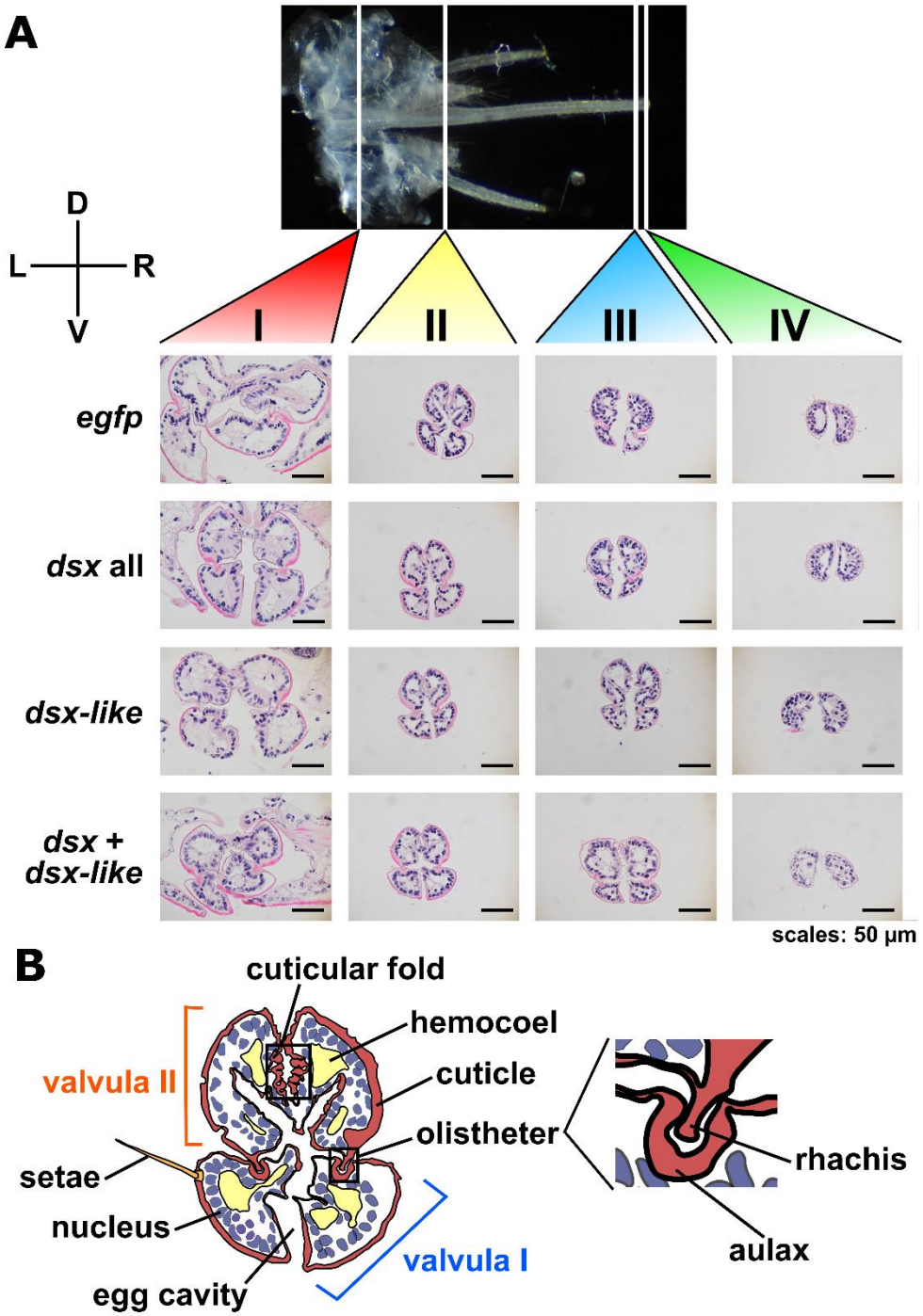

1156 **Figure 2–figure supplement 2.** Morphology of ovipositor in nymphal RNAi
1157 individuals. (A) Cross-section of the ovipositor. The photos show the morphology of
1158 the ovipositor in four parts: I (proximal part), II (middle part), III (distal part), and IV
1159 (most-distal part). D, dorsal; L, left; R, right; V, ventral. Scales: 50 μm. (B) Schematic
1160 figure of the ovipositor morphology. This figure is based on the cross-section of the
1161 part II in the control female.

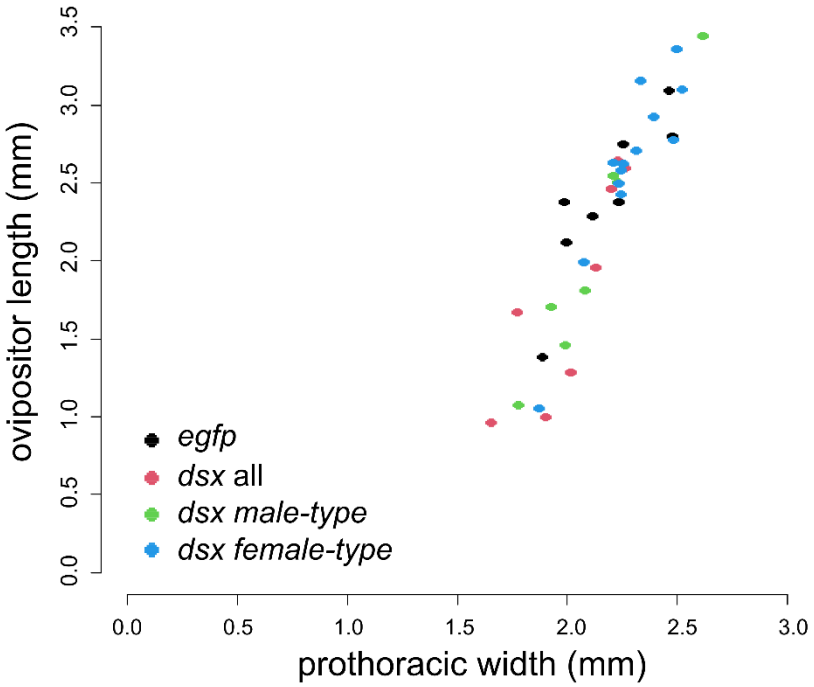

Figure 2–figure supplement 3. Ovipositor length of *dsx* isoforms RNAi individuals. The ovipositor length of *dsx* all, male-, and female-type RNAi females is plotted against the prothoracic width. The results of the statistical analysis are described in Table 4.

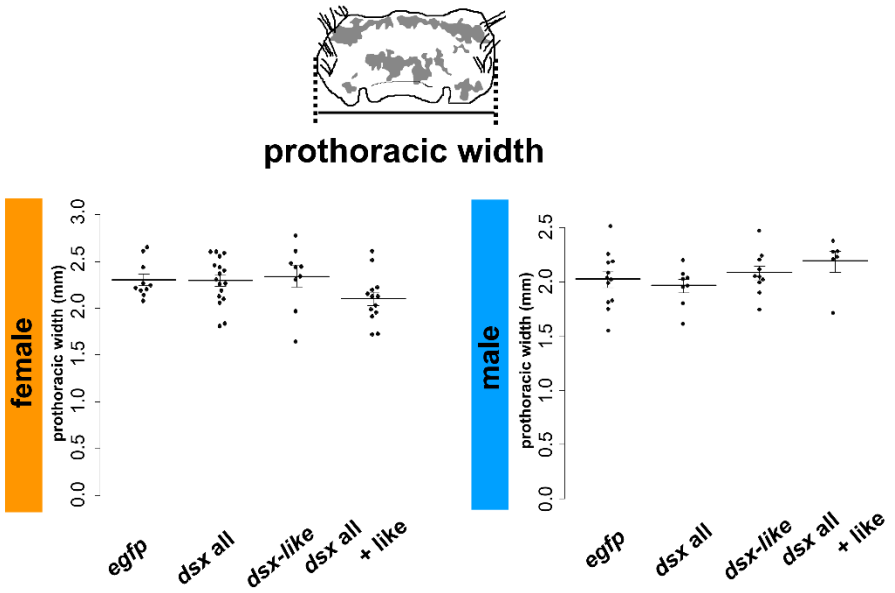

Figure 2–figure supplement 4. Prothoracic width of nymphal RNAi individuals. The left and right graphs show the female and the male size, respectively. Data shows mean ± Standard Error (SE). The results of the statistical analysis are described in Tables 4 (female) and 5 (male).

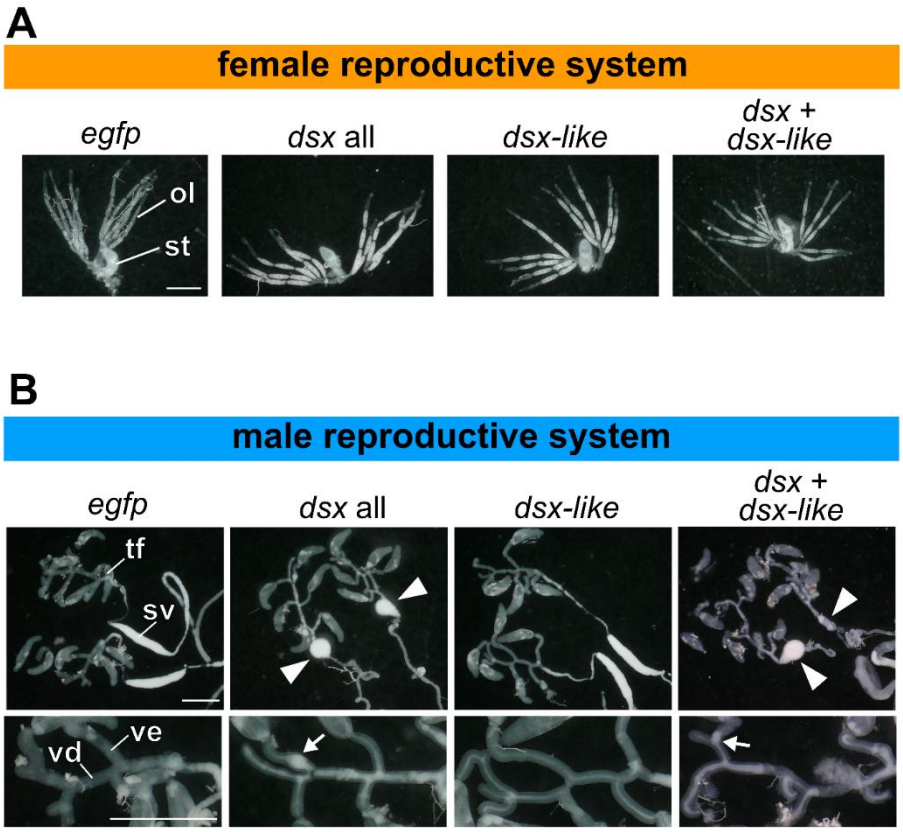

1173 **Figure 3–figure supplement 1. Gonads of nymphal RNAi individuals.** (A) female
1174 reproductive system. ol, ovariole; st, spermatheca. (B) male reproductive system. The
1175 upper photos are the are from the testicular follicle to the seminal vesicle. The lower
1176 ones are the high-magnification image of the vas efferens and the vas deferens. The
1177 arrowheads show the round-shape seminal vesicle. The arrows indicate sperm clots in
1178 the vas efferens. sv, seminal vesicle; tf, testicular follicle; ve, vas efferens; vd, vas
1179 deferens. Scales: 1 mm.

1180

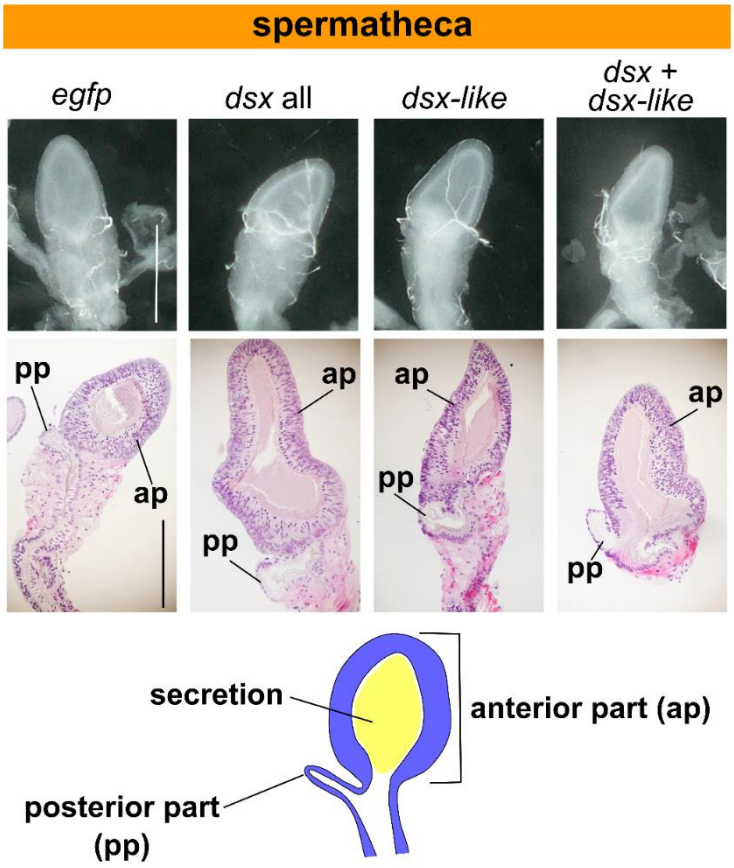

1181 **Figure 3–figure supplement 2.** Morphology of spermatheca in nymphal RNAi
1182 individuals. The upper photos show the light microscopic images of the spermatheca.
1183 The middle ones are paraffin sections of the spermatheca. The lower one is the
1184 schematic image of the spermatheca of *T. domestica*. Scales: 500 μm.

1185

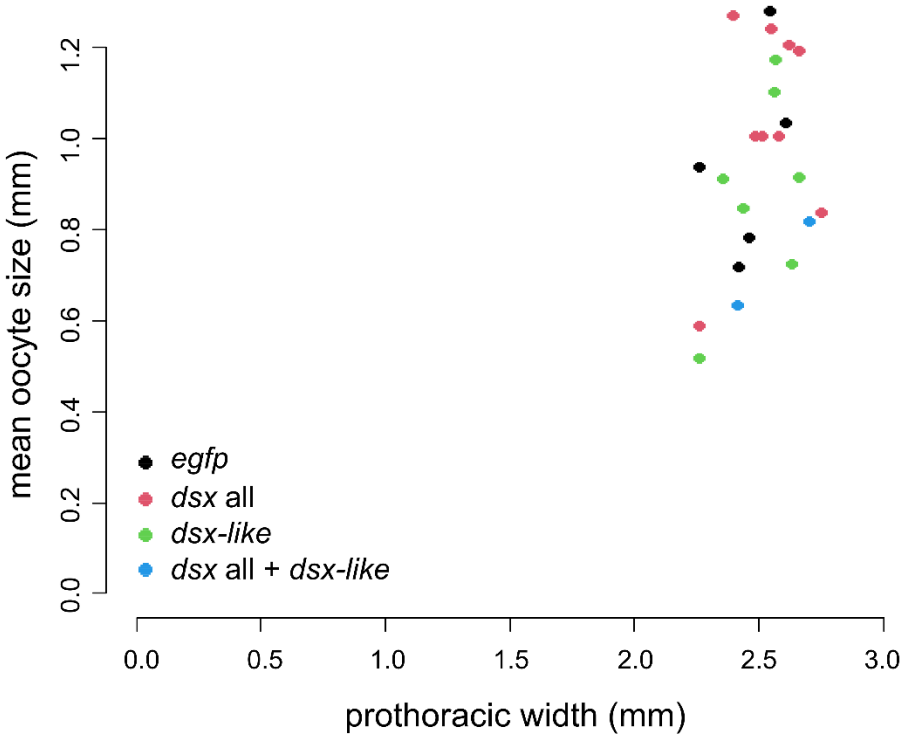

1186

1187 **Figure 3–figure supplement 3.** Oocyte size of *dsx* isoforms RNAi individuals. The
1188 oocyte size of *dsx* all, *dsx-like*, and both *dsx* and *dsx-like* RNAi females is plotted
1189 against the prothoracic width. The results of the statistical analysis are described in
1190 Table 4.

1191

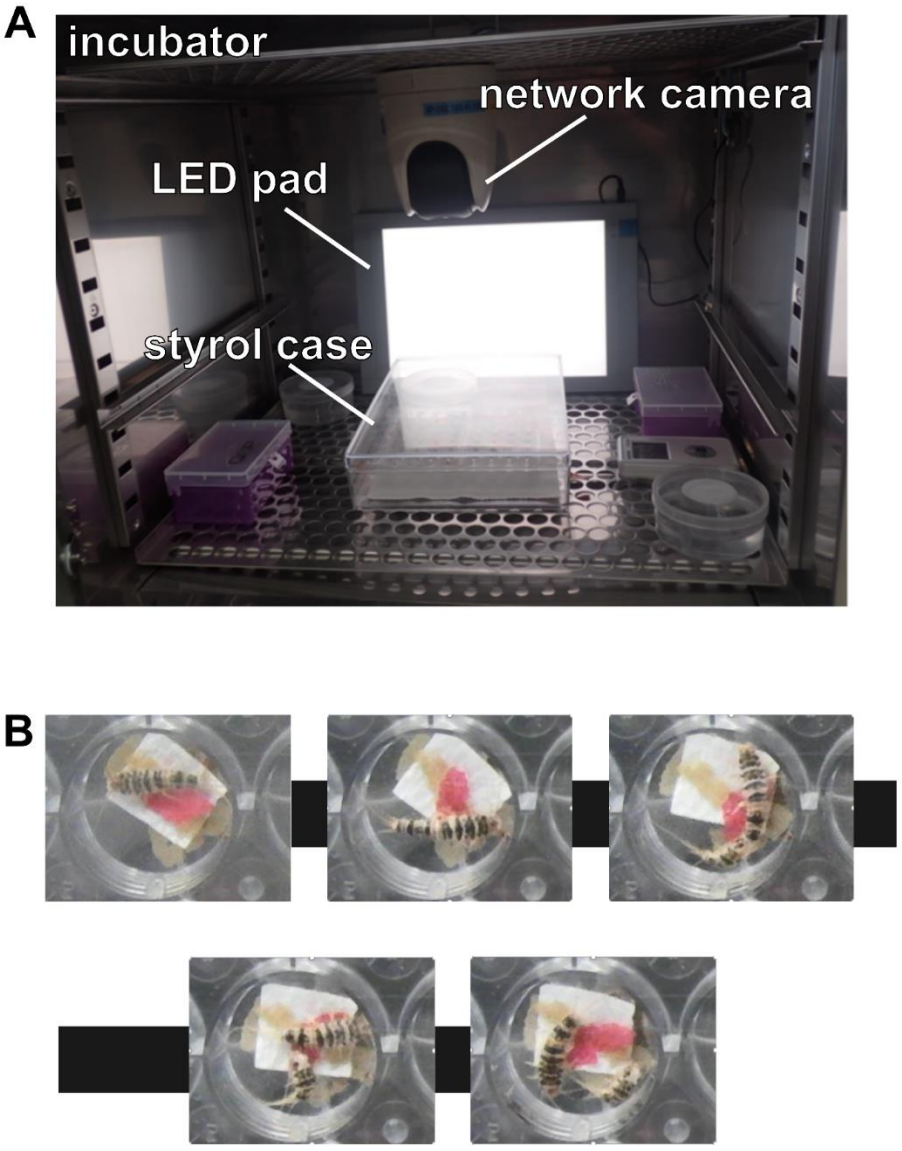

Figure 4–figure supplement 1. Time-lapse imaging system. (A) A photo of the time-lapse imaging system used to observe the molt of *T. domestica*. (B) The images during the molt.

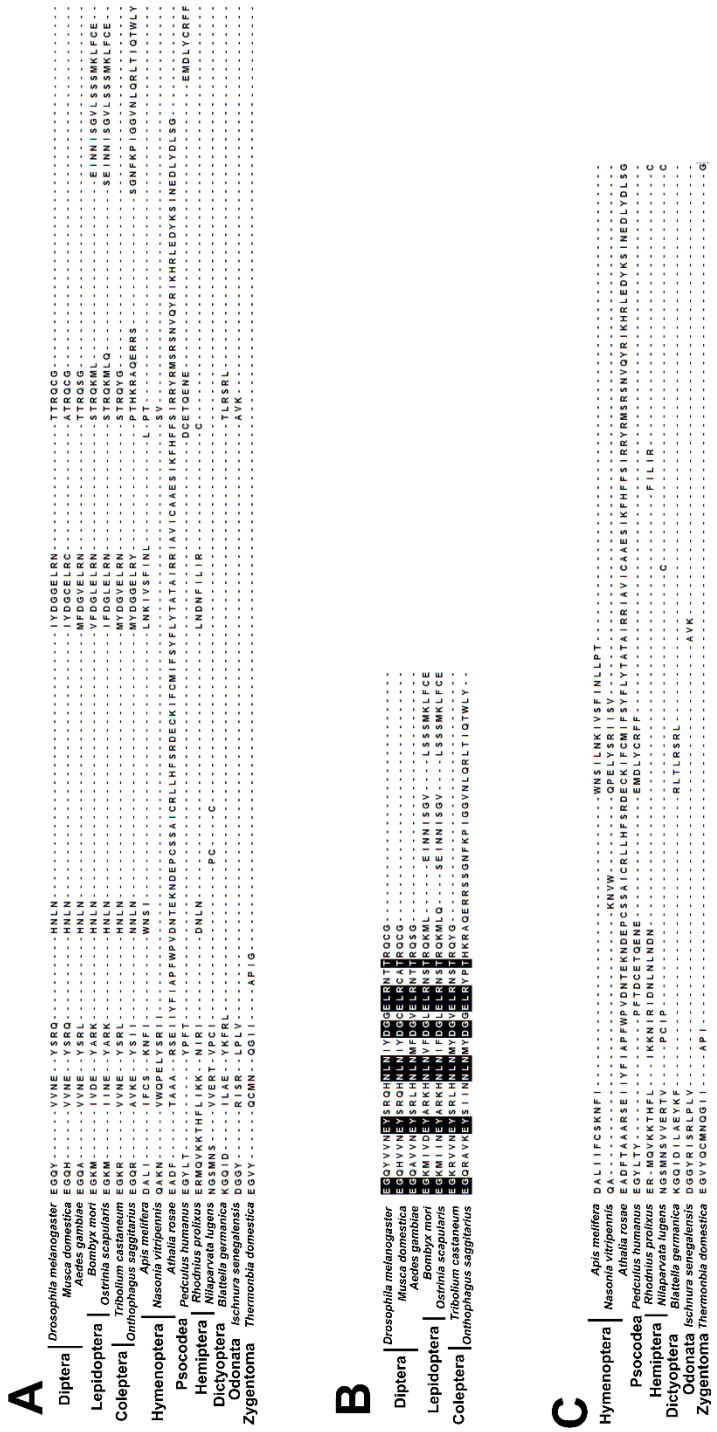

Figure 5–figure supplement 1. Multiple sequence alignments of insect Dsx female-specific region. (A) Comparison of the female-specific region of insect Dsx among the all taxa. (B) Comparison of the female-specific region of insect Dsx among the taxa with the dual-functionality. (C) Comparison of the female-specific region of insect Dsx among the taxa with the single-functionality. The black-highlighted sequences are shared in all given taxa.

Figure 5–figure supplement 2. Multiple sequence alignments of insect Dsx male-specific region. (A) Comparison of the male-specific region of insect Dsx among the all taxa. (B) Comparison of the male-specific region of insect Dsx among the taxa with the dual-functionality. (C) Comparison of the male-specific region of insect Dsx among the taxa with the single-functionality. The black-highlighted sequences are shared in all given taxa.

1210